© 2017. Published by The Company of Biologists Ltd | Development (2017) 144, 3990-4001 doi:10.1242/dev.147033

RESEARCH ARTICLE

Drosophila Atg16 promotes enteroendocrine cell differentiation via regulation of intestinal Slit/Robo signaling

Péter Nagy[1,*], Zsuzsanna Szatmári[1,*], Gyöngyvér O. Sándor[1], Mónika Lippai[1], Krisztina Hegedűs[1] and Gábor Juhász[1,2,‡]

ABSTRACT

Genetic variations of *Atg16l1*, *Slit2* and *Rab19* predispose to the development of inflammatory bowel disease (IBD), but the relationship between these mutations is unclear. Here we show that in *Drosophila* guts lacking the WD40 domain of Atg16, pre-enteroendocrine (pre-EE) cells accumulate that fail to differentiate into properly functioning secretory EE cells. Mechanistically, loss of Atg16 or its binding partner Rab19 impairs Slit production, which normally inhibits EE cell generation by activating Robo signaling in stem cells. Importantly, loss of Atg16 or decreased Slit/Robo signaling triggers an intestinal inflammatory response. Surprisingly, analysis of *Rab19* and domain-specific *Atg16* mutants indicates that their stem cell niche regulatory function is independent of autophagy. Our study reveals how mutations in these different genes may contribute to IBD.

KEY WORDS: Atg16, *Drosophila*, Inflammation, Intestine, Rab19, Slit

INTRODUCTION

Inflammatory bowel diseases (IBDs) are chronic inflammatory disorders of the gastrointestinal tract. The most common IBD forms are Crohn's disease (CD) and ulcerative colitis. Lifestyle and environment strongly influence disease progression, and several genetic risk factors are known that predispose to IBD. Although different genome-wide association studies identified multiple susceptibility loci associated with increased risk for IBD development (McGovern et al., 2015), the complex etiology of this disease is still an enigma, as the underlying molecular mechanisms and cell biological processes are poorly characterized.

The Thr300Ala (T300A) substitution in allelic variants of Atg16L1, a core autophagy protein, is a major genetic risk factor for developing CD (Hampe et al., 2007; Rioux et al., 2007). Autophagy is an evolutionarily conserved lysosomal degradation pathway of eukaryotic cells. During the main route, double-membrane autophagosomes form and subsequently fuse with endo-lysosomal vesicles to degrade their content. Atg16 (Atg16L1 in mammals) binds to a conjugate of Atg5 and Atg12, and this complex promotes Atg8/LC3 lipidation and subsequent autophagosome formation (Zavodszky et al., 2013).

Metazoan Atg16 proteins contain an Atg5-binding motif (Atg5BD) and a coiled-coil domain (CCD), which are often collectively referred to as an autophagic domain (AutD), plus a WD-repeat (WD40) domain. Both the Atg5BD and CCD are required for starvation-induced autophagy, whereas the WD40 domain mediates protein-protein interactions (Noda and Inagaki, 2015). Importantly, ubiquitin binding by the WD40 domain has been suggested to play a crucial role in selective autophagy of bacteria (xenophagy), the impairment of which is likely to be important for IBD development (Boada-Romero et al., 2016; Fujita et al., 2013; Kuballa et al., 2008).

The intestine of *Atg16l1* mutant mice contains abnormal Paneth cells, which would normally produce and secrete antimicrobial peptides to control gut microbiota and inflammation, and this was suggested to be a consequence of defective autophagic clearance of mitochondria (Cadwell et al., 2008). Paneth cells in CD patients also show elevated endoplasmic reticulum stress, which could also be due to defective autophagy (Adolph et al., 2013; Deuring et al., 2014).

In humans, the IBD-predisposing ATG16L1^{T300A} mutant protein is more sensitive to cleavage by caspase 3, possibly resulting in elevated inflammatory cytokine production and decreased antibacterial autophagy (Murthy et al., 2014). Interestingly, T300A also alters the interactions of the WD40 domain without affecting bulk autophagy (Boada-Romero et al., 2016). These data suggest that Atg16 might also have autophagy-independent functions.

The fruit fly is an excellent tool for functional analysis of genes involved in cellular and developmental processes in a complete animal. *Drosophila* intestinal homeostasis – similarly to mammals – is maintained by tightly controlled intestinal stem cell (ISC) proliferation and differentiation (Jiang and Edgar, 2012; Li and Jasper, 2016). ISCs have the unique ability to self-renew and to produce progenitor cells called enteroblasts (EBs). EBs, which are committed to either enteroendocrine (EE) or enterocyte (EC) cell fate, differentiate without further divisions into these two mature cell types of the gut. Of note, *Drosophila* EE cells simultaneously fulfill the function of human EE and Paneth cells.

Slit/Robo signaling was recently identified as a major regulator of EE cell fate commitment in *Drosophila* under homeostatic conditions. Fully differentiated EE cells secrete Slit, which acts on its receptor Robo2 (also known as Leak in *Drosophila*) that is expressed by both ISCs and differentiating precursor cells (Biteau and Jasper, 2014; Zeng et al., 2015). Activation of Robo signaling represses the homeodomain transcription factor Prospero, leading to the differentiation of EBs into EC instead of EE cells. This negative-feedback loop strictly controls the number of mature EE cells in the intestine. Importantly, EE cells promote proper gut functioning and intestinal homeostasis (Amcheslavsky et al., 2014).

Despite numerous studies on the role of Atg16 in gut homeostasis and physiology, its function in stem cell fate and in the niche has been poorly characterized. Here we analyze the effects of various Atg16 mutations in the *Drosophila* intestine. We find that the WD40 domain of Atg16 plays a crucial role in stress resistance and gut homeostasis, and its loss leads to impaired Slit/Robo-dependent

[1]Department of Anatomy, Cell and Developmental Biology, Eötvös Loránd University, Pázmány s. 1/C, Budapest, H-1117 Hungary. [2]Institute of Genetics, Biological Research Centre, Hungarian Academy of Sciences, Temesvári krt. 62, Szeged, H-6726 Hungary.
*These authors contributed equally to this work

‡Author for correspondence (szmrt@elte.hu)

G.J., 0000-0001-8548-8874

Received 15 November 2016; Accepted 25 September 2017

Development (2017) 144, 3990-4001 doi:10.1242/dev.147033

differentiation of pre-EE cells into mature secretory cells and triggers inflammation.

RESULTS

Drosophila Atg16 structure and mutations

Drosophila Atg16 is very similar to human ATG16L1 (38.2% identical, 61.1% similar amino acids) and contains a threonine (T) in the 295th position (Fig. S1), similar to human ATG16L1 T300 that is commonly substituted to alanine (A) in IBD patients. Both mammalian and fly Atg16 contain three protein domains: Atg5BD, CCD and WD40 (Fig. 1A). Atg5BD and CCD are both required for autophagy as they mediate Atg5 binding and Atg16 oligomerization (Jiang et al., 2013; Matsushita et al., 2007). The seven WD40 repeats located at the C-terminus facilitate various protein-protein interactions. The WD40 domain is dispensable for bulk autophagy in mouse embryonic fibroblasts (Fujita et al., 2009), whereas it is needed for Atg16 recruitment to bacterial phagosomes to promote xenophagy (Boada-Romero et al., 2016).

We analyzed three *Atg16* mutants: $Atg16^{d67}$ carries a large deletion that completely eliminates Atg16 protein expression; $Atg16^{d129}$ mutants lack the N-terminal Atg5BD and CCD that are required for bulk autophagy (Varga et al., 2016); and $Atg16^{MI}$ contains a Minos transposon inserted in the WD40-encoding sequence, resulting in expression of a C-terminally truncated protein (Fig. 1A). Western blots of gut protein extracts revealed that only the longest, ~70 kDa isoform of Atg16 is expressed in control flies (Fig. S2A). Atg16 is absent from $Atg16^{d67}$ mutants, and expression of genomic promoter-driven Atg16-HA is seen in genetically rescued $Atg16^{d67}$ mutants. $Atg16^{d129}$ or $Atg16^{MI}$ mutants express truncated forms of Atg16 lacking either the regions required for autophagy (Atg5BD and CCD) or part of WD40, respectively (Fig. S2A).

Alterations in Atg16 WD40 mutant flies resemble IBD

The general tissue architecture based on anti-Armadillo immunostaining and histology on transverse sections revealed no severe abnormalities in Atg^{d129} guts, whereas $Atg16^{d67}$ and $Atg16^{MI}$ intestines showed obvious morphological changes compared with control (Fig. 1B). This morphology resembled the dysplastic guts of old flies (Biteau et al., 2008), but we could not detect changes in mitotic activity or apoptosis in 5-day-old animals (Fig. S2B,C).

$Atg16^{d67}$ and $Atg16^{MI}$ posterior midguts were shorter and thicker than in wild-type flies accompanied with thickening of the epithelium, while gut diameter appeared to decrease in $Atg16^{d129}$ and $Atg7^{d77}$ (lacking the enzyme necessary for Atg8a lipidation and autophagosome formation) autophagy mutants (Fig. 1C, Fig. S2G-K). No changes were detected in food intake, peritrophic membrane thickness and cell adhesion in the various mutants tested (Fig. S2D-F), suggesting that gut integrity was not compromised.

Next, we fed the animals with dextran sodium sulfate (DSS), which is commonly used for the induction of gut inflammation in flies and mice (Amcheslavsky et al., 2009; Saitoh et al., 2008). $Atg16^{d67}$ and $Atg16^{MI}$ mutants were more sensitive to DSS treatment than Atg^{d129} mutant or control strains (Table 1). Interestingly, the burden of pathogenic bacteria [*Pseudomonas aeruginosa* (PA) and *Enterococcus faecalis* (EF)] was substantially increased in $Atg16^{d67}$ and $Atg16^{MI}$ WD40 mutant guts following oral infection (Fig. S3A). Accordingly, these flies were more sensitive to PA and EF (Table 1).

We also detected changes in the intestinal microbiota of these mutant flies. The overall number of bacteria was highly elevated in the autophagy-defective $Atg16^{d67}$ and Atg^{d129} guts (Fig. S3B), suggesting that autophagy is a major regulator of microbiota. Bacteria-specific tests revealed dramatic accumulation of Enterobacteriaceae only in $Atg16^{d67}$ and $Atg16^{MI}$ mutants (Fig. S3B), which is also frequently observed in IBD patients (Swidsinski et al., 2002). These data suggest that both autophagy and EE cells control microbes in the gut, and Atg16-dependent EE cell function might be more important for regulating a subset of bacteria and infections.

The differentiation of WD40 mutant ISCs into EE cells is impaired

Cell fate is already determined in EBs. Normally, ~90% of EBs are committed to EC specification and only ~10% of ISC progeny will become EE cells (Biteau and Jasper, 2014) (Fig. 2B). While all EBs are positive for Escargot (Esg) similar to ISCs, pre-EE cells also

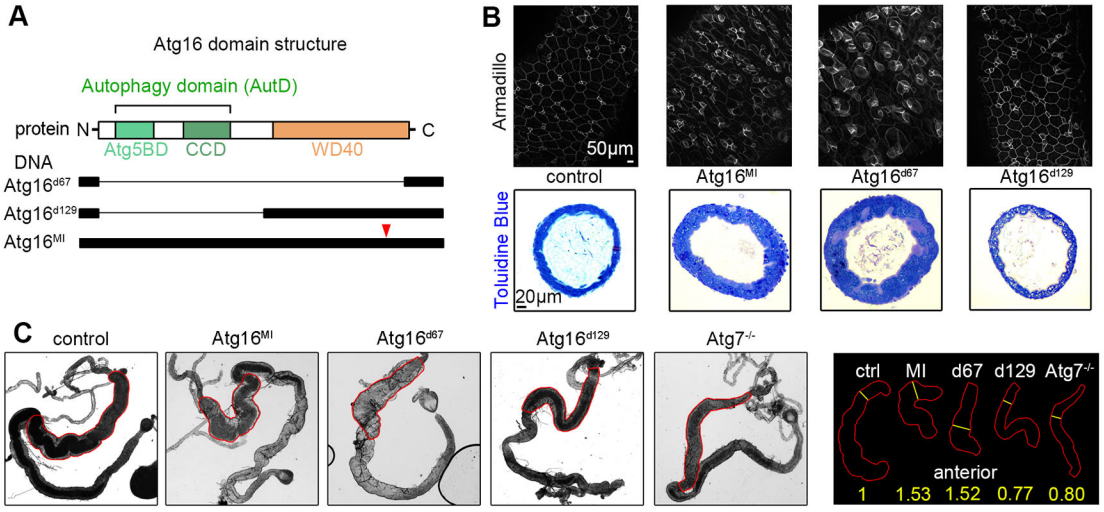

Fig. 1. Atg16 WD40 domain controls gut morphology. (A) Atg16 contains an Atg5-binding motif (Atg5BD), coiled-coil domain (CCD) and WD40 domain. The extent of deletions are indicated in the $Atg16^{d67}$ and $Atg16^{d129}$ *Drosophila* mutants. $Atg16^{MI}$ carries a Minos element in the WD40 coding region (red arrowhead marks the insertion site). (B) Posterior midgut tissue architecture is revealed by anti-Armadillo immunostaining of wild-type and *Atg16* mutant posterior midgut (top row), and in Toluidine Blue-stained histological transverse sections (bottom row). (C) Intestines of $Atg16^{d67}$ and $Atg16^{MI}$ mutants are shorter but thicker than in control or in $Atg16^{d129}$ or *Atg7* mutants. Posterior midguts are outlined in red. Numbers in the right-hand panel refer to gut diameter (relative to control set at 1) measured at the yellow lines. See Fig. S2G-I for detailed quantification of gut physical parameters. Scale bars: 50 µm (B, top row) and 20 µm (B, bottom row).

Development (2017) 144, 3990-4001 doi:10.1242/dev.147033

Table 1. Atg16 WD40 domain controls stress resistance

	DSS treatment			*Enterococcus faecalis*			*Pseudomonas aeruginosa*		
Genotype	*P*	*N*	% dead flies at day 15	*P*	*N*	% dead flies at day 5	*P*	*N*	% dead flies at day 5
Control	0.819	219	29.03	0.092	221	12.39	0.018	219	11.82
$Atg16^{d67}$	<0.001	339	43.39	<0.001	225	41.74	<0.001	229	41.53
$Atg16^{d129}$	0.977	255	31.5	0.262	222	18.97	0.194	207	17.35
$Atg16^{MI}$	0.002	366	39.83	<0.001	225	40.91	<0.001	238	37.61

$Atg16^{d67}$ and $Atg16^{MI}$ are more sensitive to DSS treatment and oral bacterial infection than control and $Atg16^{d129}$ flies. Based on Cox regression analysis. *N*, number of flies.

express Prospero (Pros) and Delta. Differentiated EE cells downregulate Esg and Delta but retain Pros expression. $Pros^+$ mature EE greatly outnumber pre-EE cells in control posterior midguts (Fig. 2C,G). The ratio of $esgGFP^+$ $Pros^+$ pre-EE versus $esgGFP^-$ $Pros^+$ mature EE cells dramatically increased in $Atg16^{MI}$ and $Atg16^{d67}$ guts, whereas it did not change significantly in $Atg16^{d129}$ mutants (Fig. 2D-G). This was also supported by Pros and Delta double labeling experiments (Fig. S4A).

We analyzed regulatory peptide expression to further explore the EE cell differentiation status in $Atg16^{d67}$ and $Atg16^{MI}$ mutants. Allatostatin C (AstC) and Diuretic hormone 31 (DH31) are highly expressed in non-overlapping subsets of mature EE cells (Beehler-Evans and Micchelli, 2015; Chen et al., 2016). There was a striking decrease in the ratio of $Pros^+$ cells expressing these regulatory peptides in *Atg16* WD40 mutant animals, and also in mutant clones (Fig. S4B-D). Timecourse analysis revealed that $Atg16^{MI}$ and $Atg16^{d67}$ mutants display delayed pre-EE maturation (Fig. S4E).

Importantly, the total number of $Pros^+$ cells also increased in $Atg16^{MI}$ and $Atg16^{d67}$ guts (Fig. S5A), in parallel with the altered pre-EE/EE ratio (see Fig. 2C-G), which was also seen in mutant clones (Fig. S5B,C). Of note, weaker effects were seen in mutant clones compared with mutant guts, suggesting that Atg16 plays a more global rather than local role in regulating EE cell generation.

To confirm the importance of the Atg16 WD40 domain for EE maturation, we carried out genetic rescue experiments by overexpressing UAS-driven transgenes (Fig. 2A) in Esg^+ stem and progenitor cells of the mutants. Overexpression of WD40 domain-containing rescue transgenes ($Atg16^{full\ length}$, $Atg16^{\Delta AutD}$ and $Atg16^{\Delta AutD+Linker}$) restored EE differentiation in $Atg16^{MI}$ and $Atg16^{d67}$ (Fig. 2G, Fig. S6E-G,I-K), whereas it had no significant effect on differentiation in the $Atg16^{d129}$ mutant (Fig. 2G, Fig. S6A-C). Overexpression of $Atg16^{\Delta WD40}$ (which lacks the WD40 domain of Atg16) had no effect on EE differentiation in these backgrounds (Fig. 2G, Fig. S6D,H,L).

ISC niche signaling is altered in Atg16 WD40 mutants

Transcriptome mapping has revealed that Atg16 is highly expressed in EE cells of the posterior midgut (Buchon et al., 2013; Dutta et al., 2015). We utilized our recently published transgenic flies expressing HA-tagged Atg16 under the control of its own genomic promoter (Varga et al., 2016) to monitor the level of Atg16 protein in different cell types of the gut. In line with the RNAseq data, we detected high Atg16 expression in $Pros^+$ and $Slit^+$ EE cells (Fig. 3A-C). Slit/Robo signaling was recently identified as a negative regulator of EE fate commitment (Biteau and Jasper, 2014; Zeng et al., 2015). Atg16 expression was lower in stem cells positive for Robo2 and Delta (Fig. 3D,E). Importantly, elevated Atg16-HA expression was already observed in $Pros^+$ $Delta^+$ and $esgGFP^+$ $Pros^+$ pre-EE cells (Fig. 3F,G).

Accumulation of pre-EE cells in *Atg16* WD40 mutant guts raised the possibility that loss of Atg16 might affect Slit/Robo signaling. Robo2 protein expression was detected in all $esgGFP^+$ cells in all genotypes (Fig. 3H-K). By contrast, Slit expression strongly decreased and showed a dramatic decline in binding to $esgGFP^+$ stem cells (that is, to its receptor Robo2) in *Atg16* WD40 mutants (Fig. 3L-O, Fig. S7A-C). qPCR experiments detected a decrease in *slit* mRNA expression in $Atg16^{MI}$ and $Atg16^{d67}$ guts (Fig. S7D), which is likely to be a consequence of impaired pre-EE cell maturation.

We carried out genetic rescue experiments to confirm the role of Atg16 and its WD40 domain in Slit/Robo signaling. Overexpression of the WD40-containing $Atg16^{full\ length}$, $Atg16^{\Delta AutD}$ and $Atg16^{\Delta AutD+Linker}$ transgenes indeed restored Slit expression and localization in $Atg16^{MI}$ and $Atg16^{d67}$ WD40 mutant guts, whereas $Atg16^{\Delta WD40}$ did not (Fig. S7E-K). Moreover, overexpression of either Slit or Robo2 in $esgGFP^+$ stem and progenitor cells restored EE differentiation in WD40 mutant flies: the ratio of pre-EE to mature EE cells was similar to that in control guts (Fig. 4A-D,I). Surprisingly, the altered localization and expression pattern of Slit observed in the absence of the Atg16 WD40 domain were rescued not only by Slit but also by Robo2 overexpression (Fig. 4E-H). It was previously shown that although impaired Slit/Robo signaling leads to increased generation of pre-EE cells, its overexpression does not suppress EE lineage commitment or differentiation on an otherwise wild-type background. It is possible that proper levels of Slit/Robo signaling also promote the differentiation of already committed pre-EE into mature EE cells (that is, more pre-EE cells form that do not properly differentiate into EE cells if Slit/Robo signaling decreases). This is supported by the expression of endogenous Robo2 protein in all $esgGFP^+$ cells (Biteau and Jasper, 2014). It is plausible that Robo2 overexpression might promote EE differentiation in *Atg16* mutants, and differentiated EE cells will produce Slit, unlike pre-EE cells that accumulate in *Atg16* WD40 mutant guts.

Finally, *esg*-specific overexpression of Robo2, Slit or the Atg16 WD40 domain in $Atg16^{d67}$ and $Atg16^{MI}$ guts restored normal tolerance to oral bacterial infection, whereas $Atg16^{\Delta WD40}$ did not (Fig. S8). These results indicate that impaired stem cell niche signaling leads to an EE differentiation defect in *Atg16* WD40 mutant guts.

Loss of Atg16 and Slit/Robo signaling induces inflammatory responses

We analyzed inflammatory responses to explore the impact of defective EE differentiation/maturation on tissue homeostasis in *Atg16* WD40 mutant intestines (Neyen et al., 2014). Upregulation of the pro-inflammatory cytokine reporter Unpaired-*lacZ* was obvious in both $Atg16^{d67}$ and $Atg16^{MI}$ mutants, whereas it remained low in control and autophagy-defective $Atg16^{d129}$ animals (Fig. 5A). Additionally, genes encoding the antimicrobial peptides Diptericin [induced by immune deficiency (IMD) pathway activation] and Drosomycin (a readout of Toll signaling) were transcriptionally upregulated in *Atg16* WD40 mutant guts (Fig. 5B). To a lesser extent, *Drosomycin* and *Diptericin* expression also increased in the

Development (2017) 144, 3990-4001 doi:10.1242/dev.147033

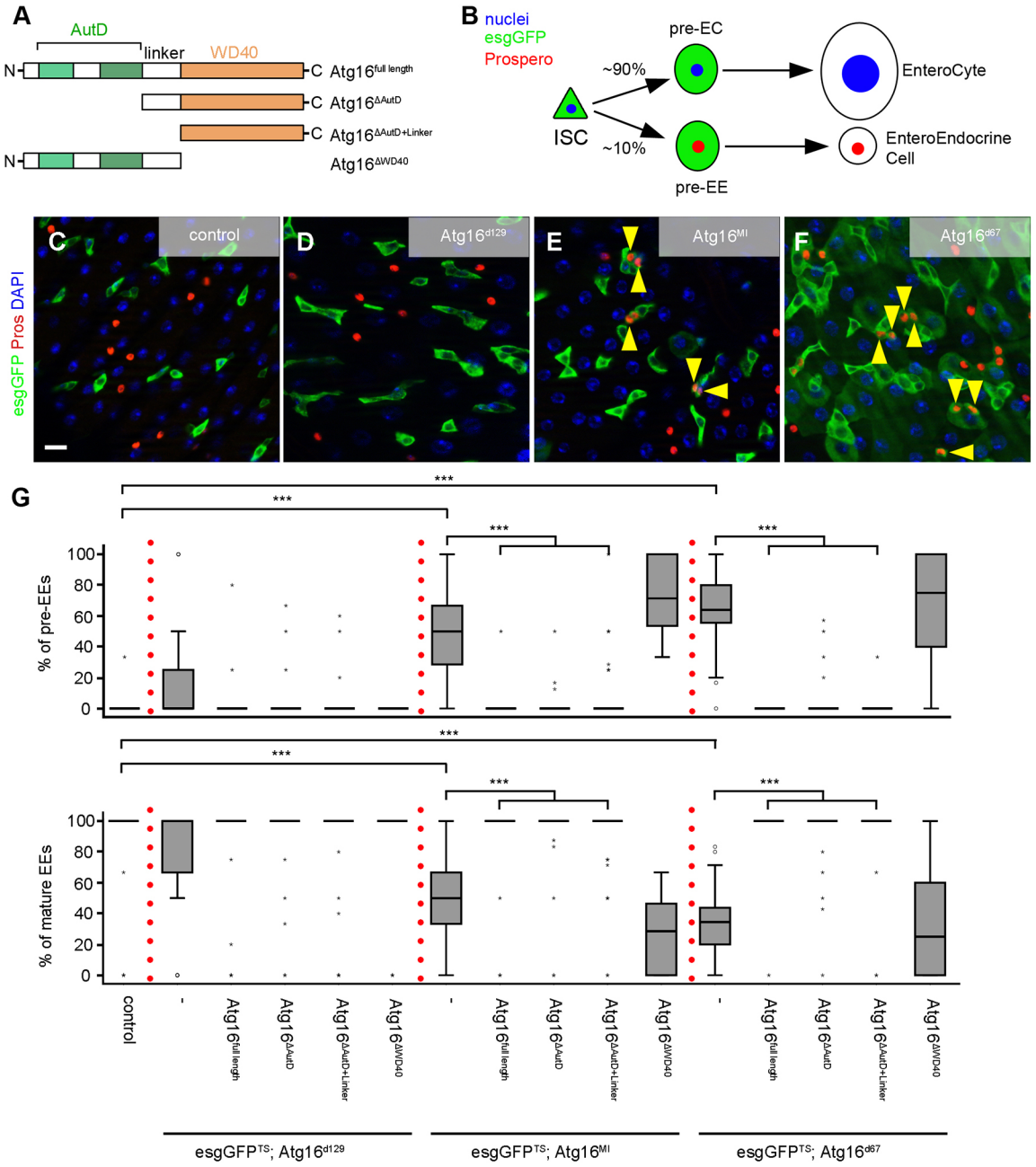

Fig. 2. EE cell differentiation requires an intact Atg16 WD40 domain. (A) Structure of the rescue transgenes/proteins used. (B) Intestinal stem cell (ISC) lineages in the adult midgut. (C-F) Esg-GFP and Pros double-positive pre-EE cells (arrowheads) accumulate in *Atg16*^{d67} and *Atg16*^{MI} guts. Esg-specific overexpression of WD40 domain-containing transgenes (*Atg16*$^{full\ length}$, *Atg16*$^{\Delta AutD}$ and *Atg16*$^{\Delta AutD+Linker}$) rescues the abnormal accumulation of pre-EE cells observed in *Atg16*^{d67} and *Atg16*^{MI}, whereas the WD40-deleted *Atg16*$^{\Delta WD40}$ does not. (G) Quantification of pre-EE versus mature EE cells. *N*=6-12. ***P<0.001 based on Kruskal–Wallis tests. Scale bar: 10 µm in C for C-F.

Atg16^{d129} autophagy mutant, suggesting that both autophagy and the Atg16 WD40 domain affect immune activity. Strikingly, these inflammatory signatures were also evident in both *robo2*$^{lea-2}$ and *slit*^{2} heterozygotes (Fig. 5C,D). Knockdown of *slit* in the Pros^{+} EE lineage was sufficient to induce an inflammatory response based on elevated *Drosomycin* and *Diptericin* expression (Fig. 5E), pointing to the importance of EE cell-derived Slit in regulating inflammation.

Autophagy status does not affect Slit/Robo signaling

Recent studies of murine IBD models suggested that impaired autophagy caused by Atg16 loss-of-function contributes to abnormalities leading to disease progression (Adolph et al., 2013; Lassen et al., 2014). We tested whether Slit/Robo signaling defects correlate with autophagy status in our various *Atg16* mutant flies. The punctate distribution of a genomic promoter-driven mCherry-Atg8a autophagy marker (Hegedűs et al., 2016) was similar in control and *Atg16*^{MI} mutant posterior midgut cells, whereas autophagy was clearly suppressed in *Atg16*^{d67} and *Atg16*^{d129} mutants (Fig. 6A-D,I). Analysis of acidic lysosomes by Lysotracker staining revealed a decrease in *Atg16*^{d67} and *Atg16*^{d129} autophagy mutants (Fig. S9A).

Ref(2)P (also known as p62) is a selective autophagy cargo, and its levels inversely correlate with autophagic degradation in *Drosophila* (Nagy et al., 2015; Nezis et al., 2008; Pircs et al., 2012). *Atg16*^{d67} and *Atg16*^{d129} mutant cells accumulated Ref(2)P

Development (2017) 144, 3990-4001 doi:10.1242/dev.147033

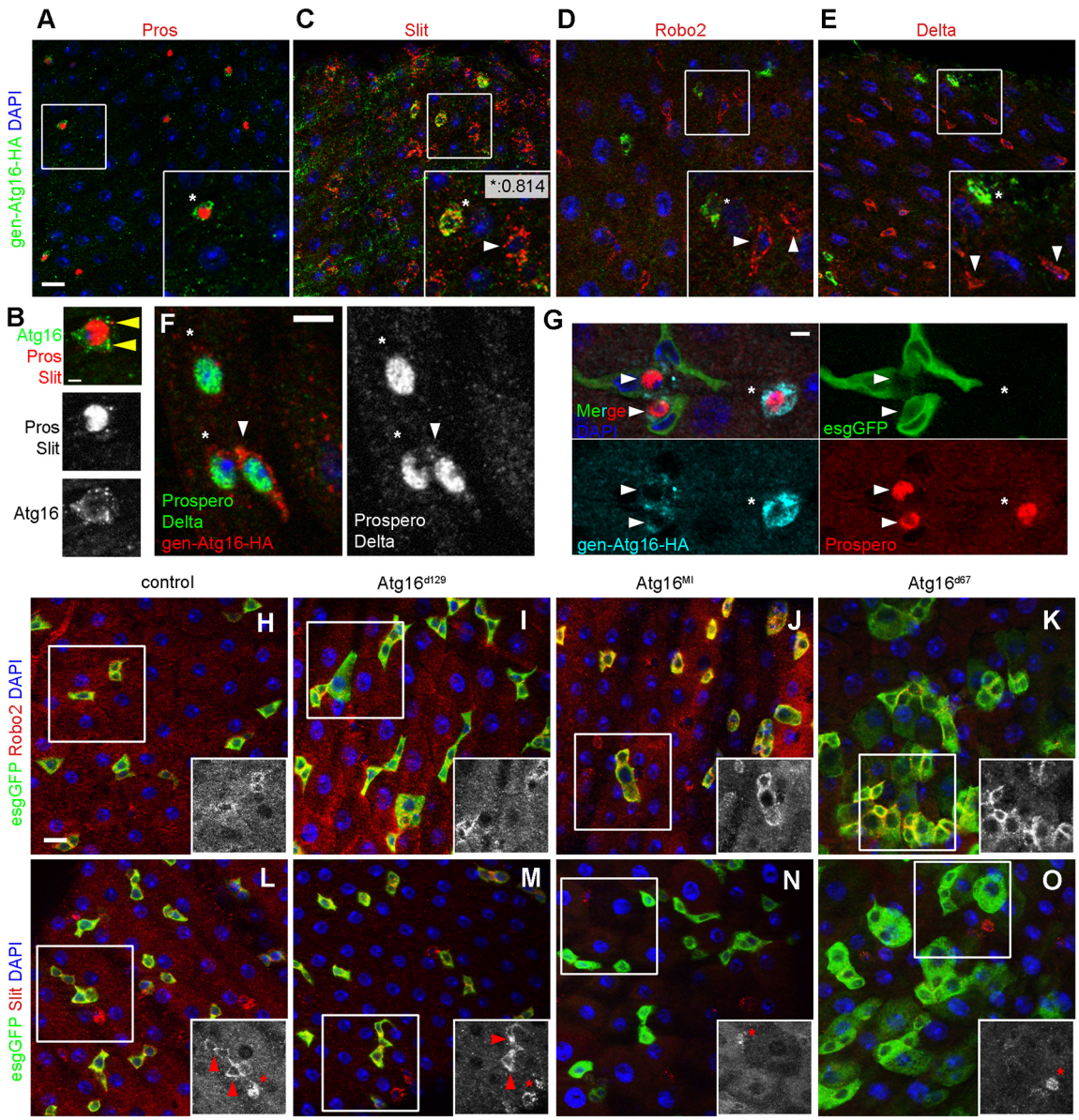

Fig. 3. ISC niche signaling is altered in Atg16 WD40 mutants. (A-E) High expression of genomic promoter-driven Atg16-HA is obvious in EE cells (asterisks) marked by Pros (A,B) and Slit (B,C), unlike in stem cells (white arrowheads) that highly express Robo2 (D) and Delta (E). Yellow arrowheads (B) point to cytoplasmic Slit expression in an EE cell with a Pros^{+} nucleus. Intensity correlation between Slit and Atg16 in the co-expressing cell (asterisk) is indicated in C. Boxed regions are enlarged in insets. (F,G) Atg16-HA is highly expressed in Pros^{+} cells that are positive/negative for Delta (F) or positive/negative for esgGFP (G). Arrowheads mark pre-EE cells and asterisks mark EE cells. (H-K) Robo2 is co-expressed with esgGFP in control and *Atg16* mutant intestines. (L-O) Slit expression declines and its localization to esgGFP^{+} stem cells observed in *Atg16*^{d129} and control guts (arrowheads) is lost in *Atg16*^{d67} and *Atg16*^{MI} mutants. Asterisks mark Slit-producing EE cells. See Fig. S7A-C for quantification of Slit expression. Scale bars: 10 µm in A,C-E,H-O; 2 µm in B,G; 5 µm in F.

aggregates, whereas its level was comparably low in control and *Atg16*^{MI} mutant intestines (Fig. 6E-I). Similarly, Ref(2)P accumulation was obvious in western blots of posterior midguts isolated from *Atg16*^{d67} and *Atg16*^{d129} mutants, and rescued by genomic promoter-driven expression of Atg16-HA (Fig. 6J). Ref(2)P mediates capture of ubiquitylated cargo into autophagosomes for selective degradation (Nezis et al., 2008; Pankiv et al., 2007). As expected, the overall level of ubiquitylated proteins was clearly increased in *Atg16*^{d67} and *Atg16*^{d129} autophagy mutants, whereas it was similar to that of the control in the *Atg16*^{MI} WD40 domain mutant and in genetically rescued *Atg16*^{d67} animals (Fig. 6J). These results indicate that the autophagic function of Atg16 is independent of its role in Slit/Robo signaling.

We also examined EE fate and stem cell niche signaling in *Atg8a* and *Atg5* null autophagy mutant flies. No alterations in Esg^{+} and/or Pros^{+} cell numbers were seen in *Atg8a* and *Atg5* mutant posterior midguts (Fig. 6K,L, Fig. S9B,C,F). Furthermore, Slit expression and its localization were not perturbed in these mutants (Fig. 6M,N, Fig. S9D,E). These findings further suggest that the Atg16 WD40 domain functions in EE differentiation independently of autophagy.

Rab19 cooperates with Atg16 to promote EE differentiation

Rab19 is a Golgi-localized Rab family protein (Sinka et al., 2008). A human *RAB19* intronic single-nucleotide polymorphism was identified as a marker of ulcerative colitis in genome-wide association studies. This allelic variant is predicted to cause copy

Development (2017) 144, 3990-4001 doi:10.1242/dev.147033

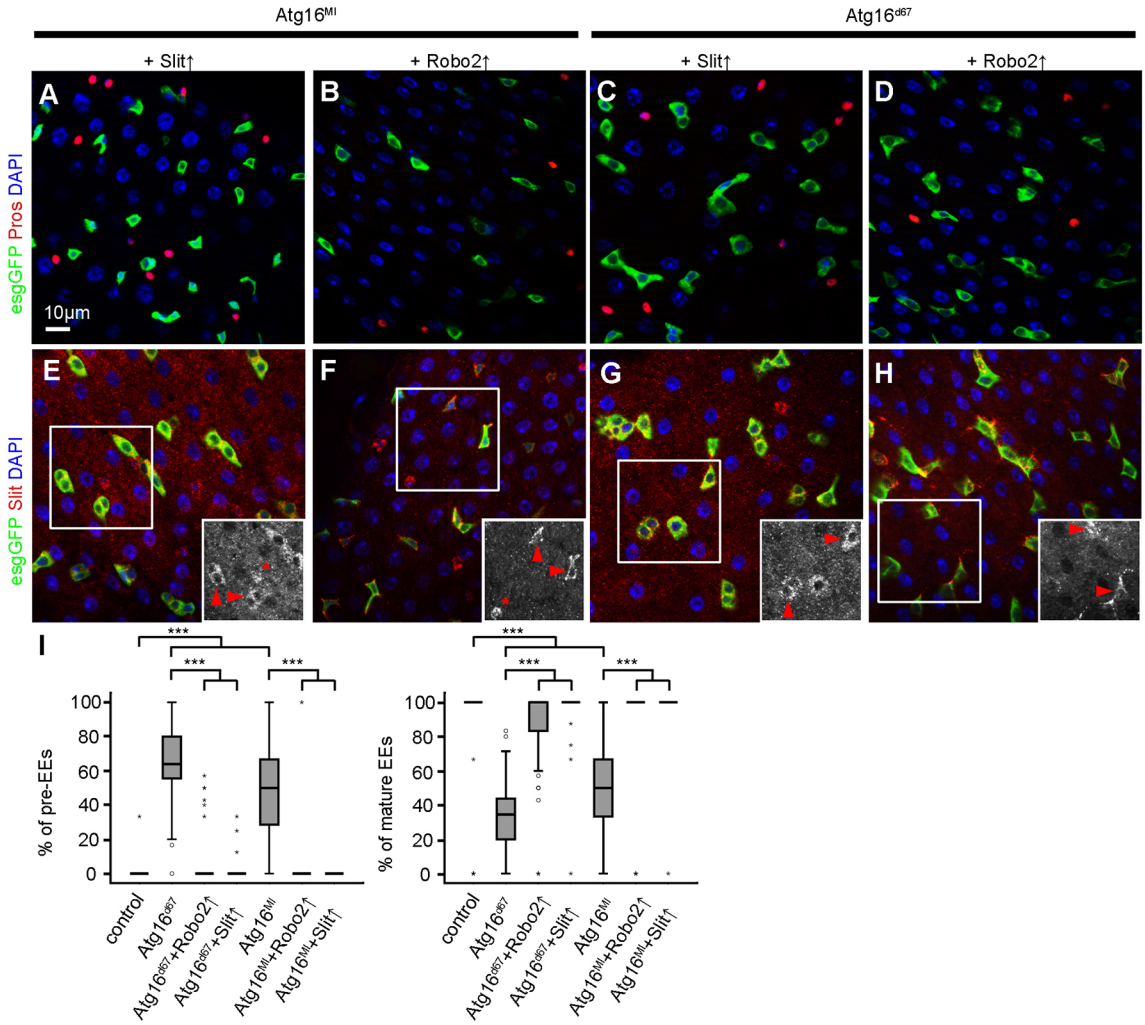

Fig. 4. Increased Slit/Robo signaling rescues the EE differentiation defect in *Atg16* mutants. Esg-specific overexpression of Slit (A,C,E,G) or Robo2 (B,D,F, H) rescues the esgGFP$^+$ Pros$^+$ pre-EE cell accumulation and esgGFP$^-$ Pros$^+$ mature EE cell decline phenotype (A-D) and restores Slit expression (E-H) in *Atg16^{d67}* and *Atg16^{MI}* guts. Arrowheads indicate esgGFP$^+$ progenitors, and asterisks mark Slit-producing EE cells. (I) Quantification of rescue data. *N*=8-12. ***P<0.001, Kruskal–Wallis tests. Scale bar: 10 μm in A for A-H.

number changes in *RAB19*, alternative splicing and loss of the start codon (Anderson et al., 2011; Coe et al., 2014), possibly resulting in RAB19 loss-of-function. This prompted us to investigate the role of Rab19 in the context of stem cell differentiation and Slit/Robo signaling in the fly intestine.

Importantly, a physical interaction between Atg16 and Rab19 was recently identified in a large-scale pull-down study (Gillingham et al., 2014). In yeast two-hybrid experiments, *Drosophila* Atg16 directly bound the active, GTP-locked form of Rab19, but did not bind GDP-locked Rab19 or the known autophagy regulators Rab2 or Rab7 (Fig. 7A) (Hegedűs et al., 2016; Lőrincz et al., 2017).

Next, we analyzed the impact of Rab19 loss on gut homeostasis and cellular composition. *Rab19* mutant flies carrying a Piggybac transposon insertion in the protein coding sequence were more sensitive to oral bacterial infection, while no autophagy defect was seen based on normal Ref(2)P and ubiquitin levels (Fig. 7B,C). Moreover, *Rab19* mutant flies contained an excess of Pros$^+$ cells in the posterior midgut (Fig. 7D). This was accompanied by decreased Slit protein and mRNA expression in *Rab19* mutant guts (Fig. 7E, Fig. S7D). These phenotypes resemble those seen in *Atg16* WD40 mutants. The impact of Atg16 and Rab19 on Slit expression was validated in a cell type-specific manner: RNAi silencing of either of these genes in Pros$^+$ cells dramatically decreased Slit expression and increased cell size (Fig. 7F-J).

Rab19-containing structures often overlapped with Atg16-HA and Slit (Fig. 7K,L), so we analyzed the relationship of Rab19 with these gene products. The subcellular distribution of Atg16-HA changed from uniform cytoplasmic to peripheral and its colocalization with Slit strongly decreased in *Rab19* mutants, further suggesting that Atg16 cooperates with Rab19 to promote EE cell generation and Slit production (Fig. 7M). This model is strongly supported by a genetic interaction between *Atg16* and *Rab19*: heterozygosity for *Rab19* together with *Atg16^{d67}* or *Atg16^{MI}*, but not *Atg16^{d129}*, led to a statistically significant increase in the total number of Pros$^+$ cells (Fig. 7N).

To confirm the role of Slit in pre-EE differentiation to EE cells, we carried out genetic epistasis analyses using Pros-Gal4. Knockdown of *Atg16* or *Rab19* in these cells impaired EE differentiation based on the decreased number of DH31$^+$ or AstC$^+$ EE cells, which was rescued by overexpression of Slit in Pros$^+$ cells (Fig. S10). Similarly, RNAi silencing of *Atg16* or *Rab19* in the Pros$^+$ EE lineage strongly increased the number of pre-EE cells co-expressing Pros and Delta, which was again rescued by overexpression of Slit (Fig. S11).

Development (2017) 144, 3990-4001 doi:10.1242/dev.147033

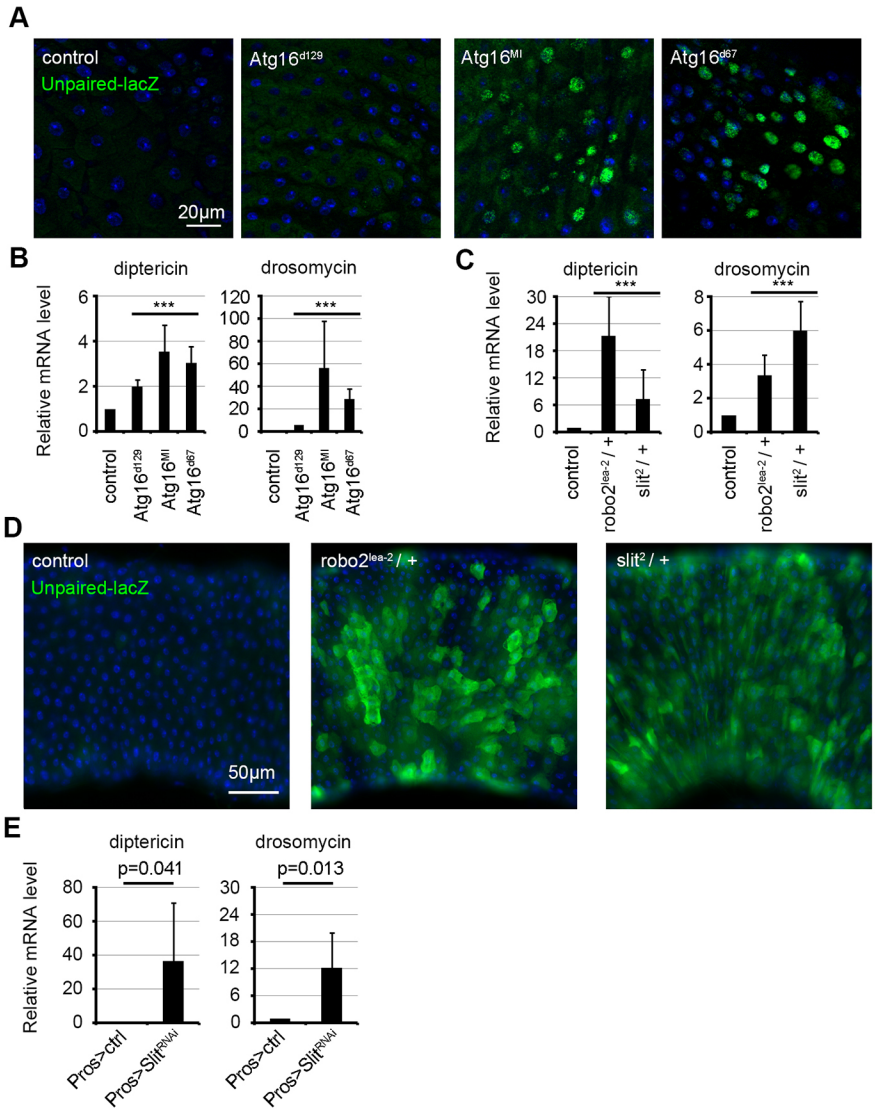

Fig. 5. Inflammatory signatures in *Atg16* homozygous mutant, *slit* and *robo2* heterozygous and EE-specific *slit* RNAi midguts. (A) Unpaired-*lacZ* expression is highly upregulated in $Atg16^{d67}$ and $Atg16^{MI}$ compared with controls, whereas $Atg16^{d129}$ mutants only display weak induction compared with controls. (B) Expression of both *Diptericin* and *Drosomycin* increase in $Atg16^{d67}$ and $Atg16^{MI}$ guts, and to a smaller extent in $Atg16^{d129}$ mutants relative to control intestines. (C) Transcriptional upregulation of *Diptericin* and *Drosomycin* is also seen in $robo2^{lea-2}$ and $slit^{2}$ heterozygotes. (D) Heterozygosity for $robo2^{lea-2}$ and $slit^{2}$ leads to Unpaired-*lacZ* induction in mutant guts. (E) Knockdown of *slit* in $Pros^{+}$ cells leads to transcriptional upregulation of *Diptericin* and *Drosomycin*. (B,C) ANOVA, ***$P<0.001$; (E) two-tailed two-sample *t*-test. Scale bars: 20 µm in A; 50 µm in D.

DISCUSSION

IBD development depends on both environmental and genetic risk factors. The T300A substitution in human ATG16L1 was identified as a major genetic risk factor for IBD (Hampe et al., 2007; Rioux et al., 2007). In this work, we show that *Atg16* loss-of-function mutations affecting the WD40 domain of the protein strongly increase the production of the pro-inflammatory cytokine Unpaired in the midgut, and the sensitivity to the colitis-inducing drug DSS. This is similar to the increased DSS sensitivity and high IL1β inflammatory cytokine production observed in *Atg16l1* mutant mice (Saitoh et al., 2008). Interestingly, *Drosophila Atg16* WD40 domain mutants are especially sensitive to infection by PA and EF, while all three alleles of *Atg16* (autophagy-specific $Atg19^{d129}$, WD40-specific $Atg16^{MI}$, and the null $Atg16^{d67}$) lead to increased antimicrobial peptide production, with the null allele producing the strongest phenotypes. Given that the T300A polymorphism causes increased cleavage by caspase 3 and downregulation of ATG16L1 expression in human and mouse cells (Murthy et al., 2014), we think that among our mutants, $Atg16^{d67}$ is the best to model the disease in flies. Alterations in gut flora are also detected in all *Atg16* mutant flies, similar to the perturbed commensal microbiota in IBDs (Huttenhower et al., 2014; Sartor, 2008). Thus, *Atg16* mutant flies recapitulate several symptoms observed in IBD patients and mouse models.

Proper homeostasis of the intestinal tract enables gut epithelia to absorb nutrients and to defend against pathogens by maintaining the immunological barrier (Li and Jasper, 2016). This balance depends on the tightly regulated proliferation and differentiation of stem cells and progenitors. The mammalian gut is composed of three types of secretory cells: the hormone-producing EE cells, mucus-producing goblet cells and the antimicrobial peptide-producing Paneth cells. The epithelium of the *Drosophila* posterior midgut contains only one type of secretory (EE) cell, which fulfills the function of both of the mammalian EE and Paneth cells. In mammals, Paneth cells also provide a niche and signals for $Lgr5^{+}$ stem cells in intestinal crypts (Sato et al., 2011), similarly to fly EE cells that may produce Slit to control lineage specification of progenitors (Biteau and Jasper, 2014; Zeng et al., 2015). Our work revealed that pre-EE cells accumulate as a consequence of *Atg16* WD40 domain and *Rab19* mutations. These atypical cells fail to produce enough Slit (an inhibitor of EE cell fate) as inferred from its decreased mRNA and protein levels (Fig. S7C,D), which may lead to an accumulation of more pre-EE cells. It is possible that Atg16 and Rab19 also play a more direct role in Slit trafficking or stability based on the

Development (2017) 144, 3990-4001 doi:10.1242/dev.147033

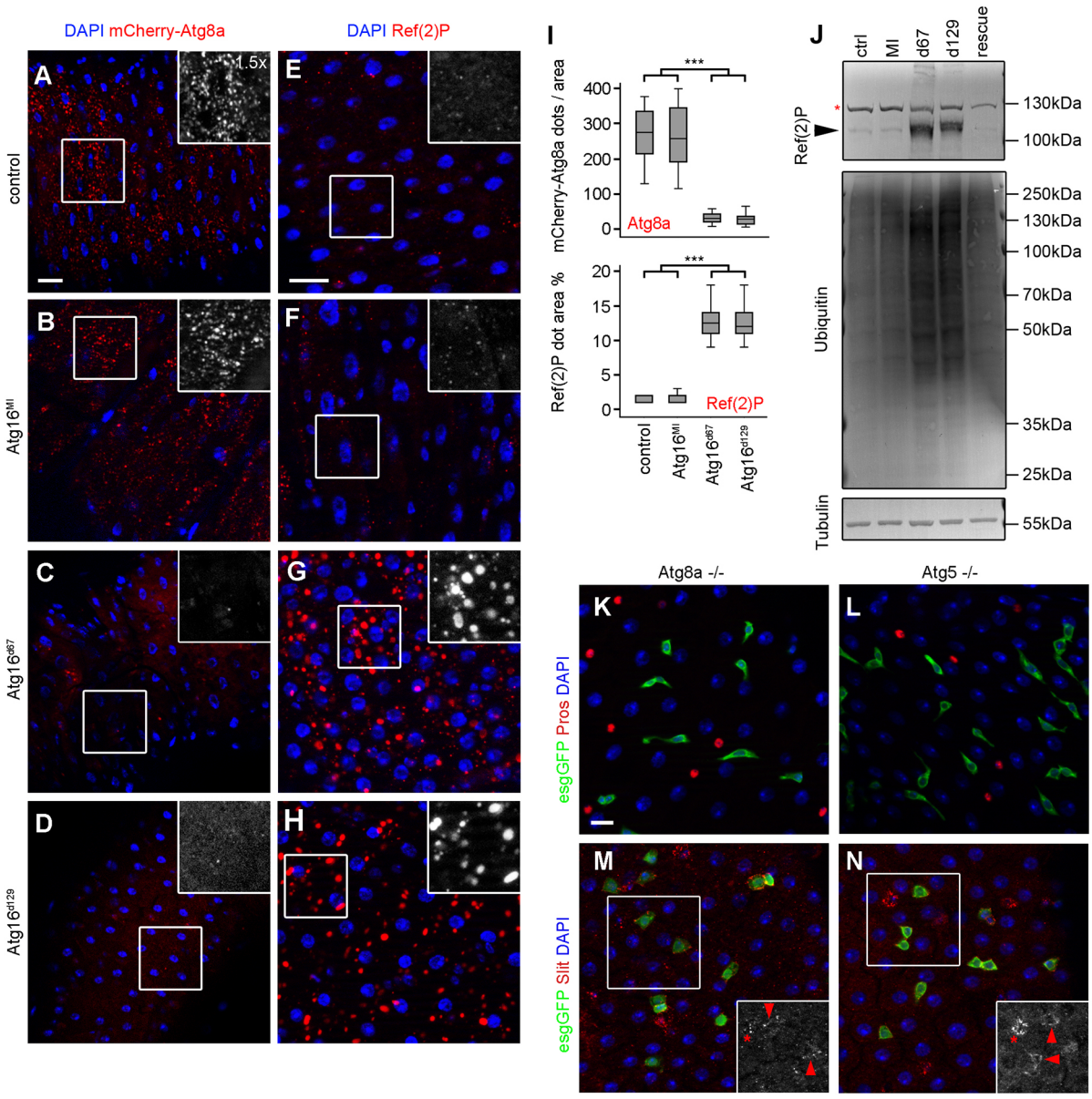

Fig. 6. Autophagy status does not influence Slit/Robo signaling. (A-I) The number of mCherry-Atg8a^{+} autophagic vesicles in *Atg16*^{MI} guts is similar to that in controls, whereas a strong reduction in its punctate localization is observed in *Atg16*^{d129} and *Atg16*^{d67} mutants (A-D). Accumulation of the autophagic cargo Ref(2)P is striking in *Atg16*^{d129} and *Atg16*^{d67} midguts compared with control and *Atg16*^{MI} animals (E-H). (I) Quantification of the Atg8a and Ref(2)P data. *N*=10-13. ***P<0.001 based on ANOVA (Atg8a) and Kruskal–Wallis [Ref(2)P] analyses. (J) Western blot reveals that Ref(2)P and ubiquitylated proteins accumulate in *Atg16*^{d129} and *Atg16*^{d67} midguts relative to control and *Atg16*^{MI} mutants. Autophagic cargo clearance is rescued in *Atg16*^{d67} mutants by expression of genomic promoter-driven Atg16-HA. The asterisk marks a non-specific band. (K-N) *Atg8a* and *Atg5* mutant midguts do not show abnormal esgGFP^{+} Pros^{+} pre-EE cell accumulation (K,L) and Slit expression/localization defects (M,N). Arrowheads and asterisks mark ISCs and EE cells, respectively. See Fig. S9B-F for genotype controls and quantification of pre-EE cells. Scale bars: 50 µm in A-D; 20 µm in E-H; 10 µm in K-N.

overlapping distribution of these proteins, and the requirement of Rab19 for the colocalization of Atg16 and Slit.

A recent paper challenged the model of EE cell density regulation by locally produced Slit, because knockdown of *slit* in randomly generated midgut cell clones did not affect EE cell numbers (Sallé et al., 2017). Possibly, Slit is highly diffusible and its overall level in the midgut controls EE cell generation, since it was confirmed that Pros^{+} cell numbers increase upon *slit* knockdown by EE lineage-specific drivers (Biteau and Jasper, 2014; Sallé et al., 2017). In line with this, we observed stronger phenotypes in guts of animals lacking the Atg16 WD40 domain or in EE-specific *Atg16* knockdown experiments as compared with *Atg16* mutant clones.

Dysregulated niche signaling during IBD is supported by decreased frequency of organoid formation of wild-type Lgr5^{+} murine stem cells co-cultured with Paneth cells carrying Atg16L1^{T300A} or another Atg16L1 mutation (Lassen et al., 2014). In addition, aberrant niche signaling was observed in human IBD patients (Kini et al., 2015), in line with the Paneth cell abnormalities observed in hypomorphic *Atg16l1* mutant mice and in human patients carrying the *ATG16L1* risk allele (Cadwell et al., 2008).

Humans harboring genetic variations of *ATG16L1* (Hampe et al., 2007; Rioux et al., 2007), *SLIT2* (Azuara et al., 2013; Lobatón et al., 2014) and *RAB19* (Anderson et al., 2011; Coe et al., 2014) have an increased risk of developing IBD, but the possible interaction between

Development (2017) 144, 3990-4001 doi:10.1242/dev.147033

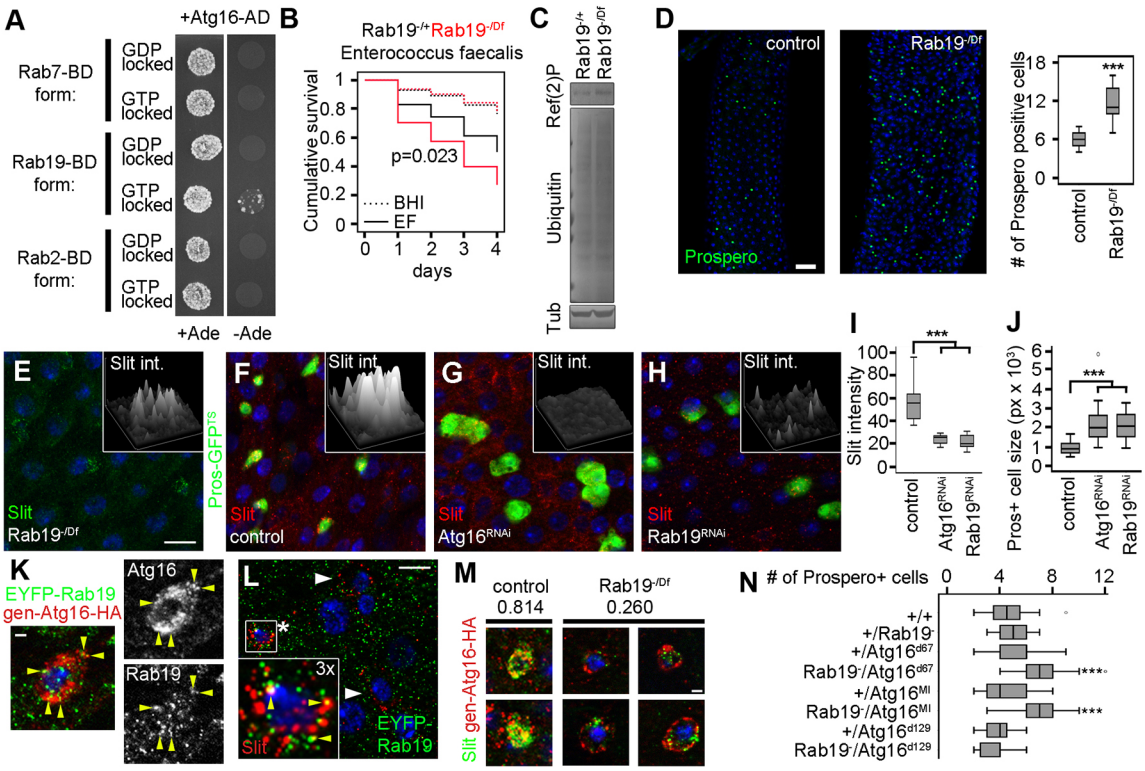

Fig. 7. Rab19 cooperates with Atg16 in Slit production and EE differentiation. (A) Yeast two-hybrid analysis reveals that Atg16 directly binds to the active, GTP-locked form of Rab19, but not to its inactive, GDP-locked form or to Rab7 or Rab2. (B) *Rab19* mutant animals are more sensitive to oral *Enterococcus faecalis* (EF) infection than control (BHI, brain heart infusion medium) flies based on Cox regression analysis. *N*=268-366. (C) No accumulation of Ref(2)P and ubiquitylated proteins is seen in western blots of *Rab19* mutant guts. (D) The number of Pros^{+} cells increases in *Rab19* mutants. *N*=18. ***P<0.001, two-tailed two-sample *t*-test. (E) Slit expression decreases in *Rab19* mutant cells. (F-J) Compared with controls (F), knockdown of *Atg16* (G) or *Rab19* (H) in Pros^{+} cells impairs Slit production as quantified in I (*N*=10; ANOVA, ***P<0.001) and alters cell size as quantified in J (*N*=30; ANOVA, ***P<0.001). (K-M) YFP-Rab19 signal overlaps with Atg16-HA (K) and endogenous Slit (L). Yellow arrowheads indicate colocalization (K,L), and white arrowheads and asterisks point to Slit^{+} stem and EE cells, respectively (L). Mutation of *Rab19* disrupts Atg16-HA and Slit colocalization (numbers indicate Pearson correlation coefficients in the selected cells) and leads to peripheral distribution of Atg16-HA dots (M). (N) Genetic interaction analysis using various *Atg16* and *Rab19* single and transheterozygous mutant flies. *N*=10. ***P<0.001, Kruskal–Wallis test. Scale bars: 50 µm in D; 20 µm in E-H; 2 µm in K,M; 10 µm in L.

these factors is unknown. Slit levels dramatically decrease in the midgut of *Atg16* WD40 and *Rab19* mutant flies, similar to IBD patients with decreased Slit expression due to promoter hypermethylation (Lobatón et al., 2014). Interestingly, Slit promoter hypermethylation in IBD patients is associated with an increased risk of cancer (Carmona et al., 2013). Notably, Atg16 WD40 mutations also lead to an early dysplasia-like gut phenotype in adult flies.

Dysplasia might potentiate the development of pre-cancerous intestinal lesions in mammals (Li and Jasper, 2016). This is consistent with the elevated risk of IBD patients to develop colorectal cancer (Ekbom et al., 1990). Human patient data also suggest that bulk autophagy is not perturbed in colorectal cancer cells carrying the ATG16L1 T300A variant, while the level of type I interferon is highly elevated and improves survival (Grimm et al., 2016). These findings support a proposal that the differentiation and proper functioning of *Atg16* mutant EE/Paneth cells does not depend on bulk autophagy.

Taken together, we show that Atg16 and Rab19 cooperatively promote secretory cell differentiation and Slit production, a determinant of EE fate specification. Importantly, loss of Atg16 and decreased Slit/Robo signaling lead to an inflammatory response characterized by increased inflammatory cytokine expression and activation of IMD and Toll immune pathways (Fig. 8). Thus, impairment of stem cell niche signaling might also contribute to IBD development in human patients.

MATERIALS AND METHODS

Fly husbandry

Drosophila stocks and crosses were maintained on standard cornmeal/sugar/agar medium at 22°C. Gene/RNAi expression was induced by shifting vials containing adult flies to 29°C. Stocks used were: *gen-Atg16-HA*, *Atg16^{d67}*, *Atg16^{d129}*, *UAS-Atg16$^{full\ length}$* (Varga et al., 2016), *Atg16^{MI00187}*, *Atg7$^{d77/d14}$* (Juhasz et al., 2007), *esgGFP^{TS} [esg-Gal4, UAS-GFP, Tub-Gal80^{ts}]*, *slit^{EY10695}*, *robo2/Lea^{EP17071}*, *UAS-slit RNAi^{JF01229}*, *slit^{2}*, *robo2^{lea-2}* (Biteau and Jasper, 2014), *Atg8a^{KG07569}*, *Atg5^{5CC5}* (Kim et al., 2016), *gen-mCherry-Atg8a* (Hegedűs et al., 2016), *UAS-Atg16$^{\Delta AutD}$*, *UAS-Atg16$^{\Delta AutD+Linker}$*, *UAS-Atg16$^{\Delta WD40}$* (all three generated in this study), *UAS-Atg16 RNAi [HMS01347]*, *UAS-Rab19 RNAi [HMS00592]*, *Rab19[EYFP]*, *Df(3L) BSC815*, *Rab19^{LL00490}* (Schuldiner et al., 2008), *prosperoGFP^{TS}* (*Tub-Gal80^{ts}, UAS-GFP; pros^{V1}-Gal4*), *unpaired-lacZ* (Jiang et al., 2009).

Culture medium was supplemented with 5% Bromophenol Blue for gut leakage analysis. Gut clearance and food uptake assays were carried out as described (Amcheslavsky et al., 2014). Mutant clones were generated by somatic recombination using the MARCM stock *hsFlp; Tub-Gal4, UAS-GFP; FRT82B Tub-Gal80*. Virgins were crossed with *FRT82B Atg16* mutant lines. 3- to 5-day-old mated female flies were heat shocked for 40 min at 37°C. Flies were transferred to 25°C and clones were analyzed 11 days after heat shock-induced somatic recombination.

Survival analyses

During these experiments, flies were kept at 25°C. For DSS treatment, 3 h-starved 5-day-old flies were transferred to sterile vials containing 2.5×3.5 cm pieces of Whatman paper and 900 µl 3% DSS in 5% sucrose

Development (2017) 144, 3990-4001 doi:10.1242/dev.147033

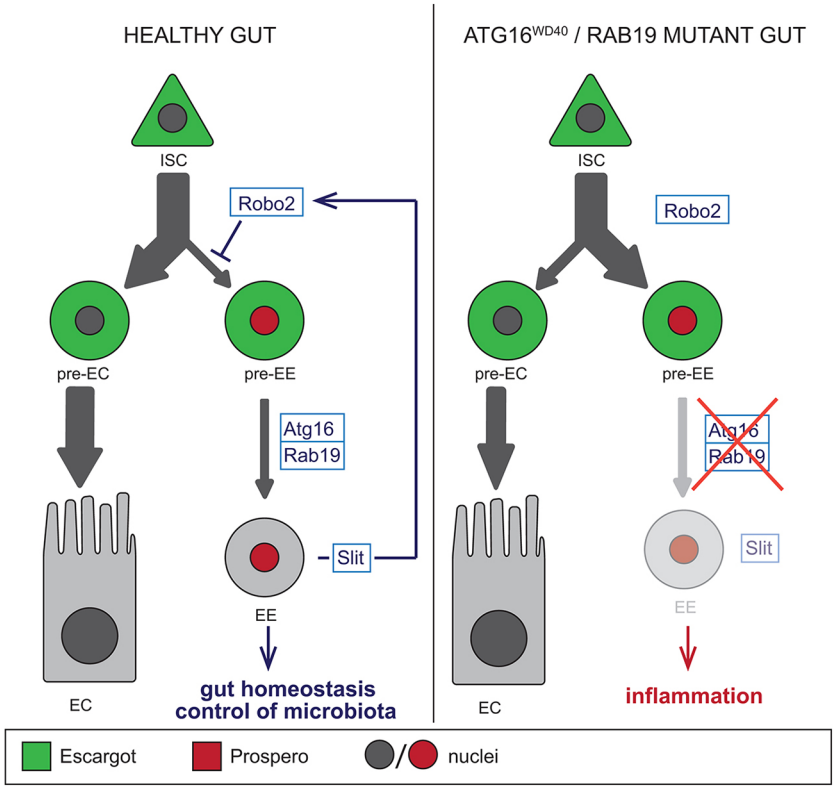

Fig. 8. Impaired ISC niche signaling and EE differentiation in *Atg16* WD40 and *Rab19* mutants promotes the emergence of inflammatory signatures. The cellular composition of midguts is altered in *Atg16* WD40 and *Rab19* mutants: the accumulation of pre-EE cells is accompanied by a decline in mature EE cells and decreased Slit production. This leads to elevation of inflammatory responses, including the transcriptional upregulation of the inflammatory cytokine Unpaired and the antimicrobial peptides Diptericin and Drosomycin, which are indicators of IMD and Toll immune pathway activation, respectively.

or, in control groups, 5% sucrose solution. After 3 days of treatment, flies were transferred to standard agar/cornmeal medium and the number of dead animals was monitored daily.

Isogenic strains of *Enterococcus faecalis* (EF) and *Pseudomonas aeruginosa* (PA14) were used to infect flies. PA14 was cultured in Luria-Bertani (LB) medium and EF in brain heart infusion (BHI) medium at 37°C. Infection procedures were adapted from a previously published fly-feeding assay (Chugani et al., 2001). Experiments were carried out using 20 male and 20 female flies per vial. After 3 h starvation, 5-day-old flies were transferred to sterile vials containing 2.5×3.5 cm pieces of Whatman paper and 900 µl LB or BHI medium in the presence or absence of bacterial strains. Both cultures were grown overnight at 37°C, and 5% sucrose was added. Flies were transferred to fresh medium twice a week and the number of dead animals counted each day. At the end of lifespan experiments, the cumulative survival ratio was calculated for each group, and the survival probability of flies exposed to DSS or bacterial infection and their counterparts maintained on sucrose solution was analyzed.

Quantification and statistical analysis

Images were analyzed with ImageJ (NIH). We counted the number of $Pros^+$, Esg^+, $AstC^+$, $DH31^+$ or double-positive cells in the posterior midgut using 473×473 pixel sampling quadrats in images taken with a 40× objective. Images from at least ten flies per group were quantified. To randomize our sampling method, we selected the position for the upper left corner of quadrats by generating random *x* and *y* coordinates with uniform distribution using Microsoft Excel. We used only the coordinates that specified quadrats containing gut tissue only. We counted all of the cells positive for the markers in the quadrat even if the quadrat did not contain the whole cell. Percentage of EBs was calculated using the formula: [(number of Esg^+ $Pros^+$ double-labeled cells)/(number of $Pros^+$ cells)]×100. The number of phospho-histone $H3^+$ cells was counted in each image showing regions of posterior midgut taken with a 10× objective. Slit intensity was analyzed and surface plots were generated using ImageJ.

Statistical analysis was performed in SPSS 21 (IBM) using the indicated tests based on first checking for normality of data distribution. Box plots, which were also generated using this software, show the data lying between the upper and lower quartiles, with the median indicated as a horizontal line within the box; whiskers plot the smallest and largest data observed, and dots indicate outliers. $P<0.05$ was considered significant. Two-tailed, two-sample *t*-tests were used for pairwise comparison in the case of two samples, and Kruskal–Wallis and ANOVA tests were used to calculate *P*-values for multiple comparisons; Hochberg and Bonferroni post-hoc tests were carried out for multiple comparisons to reduce type II errors in ANOVA and Kruskal–Wallis analyses, respectively.

Western blot

Western blotting was carried out as described (Nagy et al., 2013). Briefly, 20 guts were isolated and homogenized in Laemmli sample buffer (Sigma) containing aprotinin, leupeptin and PMSF to avoid protein degradation. Primary antibodies were rat anti-Atg16/1 (1:5000) (Varga et al., 2016), rabbit anti-p62 (1:5000) (Pircs et al., 2012), rabbit anti-ubiquitin (1:500; DAKO, Z0458) and mouse anti-α-tubulin (1:1000; DSHB, AA4.3-s). Secondary antibodies were alkaline phosphatase-conjugated goat anti-rat, anti-rabbit and anti-mouse (1:5000; Millipore).

Immunostaining and microscopy

Tissue isolation, fixation, preparation, labeling and fluorescent and electron microscopy were carried out as described (Nagy et al., 2013, 2016). Primary antibodies used were rabbit anti-p62 (1:2000) (Pircs et al., 2012), chicken anti-GFP (1:1500; Invitrogen, A-10262), mouse anti-Delta (1:100; DSHB, C594.9B), mouse anti-Slit (1:100; DSHB, C555.6D), rabbit anti-phospho-histone H3 (1:300; Millipore, 06-570), mouse anti-Armadillo (1:50; DSHB, N2 7A1), mouse anti-Prospero (1:100; DSHB, MR1A), rat anti-mCherry (1:300) (Takáts et al., 2013), rabbit anti-HA (1:50; Sigma-Aldrich, H6908), mouse anti-β-galactosidase (1:100; DSHB, 40-1a), rabbit anti-Allatostatin C and rabbit anti-DH31 [both 1:200; kindly provided by Jan Veenstra (Veenstra et al., 2008)]; and secondary antibodies (all 1:1500; Invitrogen) were Alexa Fluor 488 anti-chicken (A11039), Alexa Fluor 586 anti-rabbit (A11036), Alexa Fluor 568 anti-mouse (A11031), Alexa Fluor 647 anti-rabbit (A21245) and Alexa Fluor 568 anti-rat (A11077).

Yeast two-hybrid assay

Atg16 (IP15590) EST was amplified using primers (5′-3′): ATGTCTACG-GAGGAGCATGTGTGG and CTATGACTCCGAGTAGATGGTGCAG-

Development (2017) 144, 3990-4001 doi:10.1242/dev.147033

CG. Constitutively active and dominant-negative Rab19 were amplified using genomic DNA template from transgenic fly stocks with primers: ATGACCGCCCGCAATCCT and CTAGGTGAGATTGCATGAGCTGC. The fragments were cloned into pGADT7 AD (Gal4 DNA-activation domain) and pGBKT7 BD (Gal4 DNA-binding domain) vectors (Clontech) and then transformed into the yeast strain PJ69-4A using the Frozen-EZ Yeast Transformation II Kit (Zymo). The GTP-locked and GDP-locked versions of Rab2 and Rab7 were as described (Lőrincz et al., 2017). Transformed cells were selected based on growth in minimal medium (Trp^-, Leu^-) and reporter gene activation was assessed by growth on Trp^-, Leu^-, Ade^- plates, with empty vectors as negative controls. At least three colonies were checked for interaction in each transformation (Hegedűs et al., 2016).

Quantitative PCR (qPCR) analyses

RNA was extracted from 15 midguts per genotype using the Direct-zol RNA MiniPrep Kit (Zymo), which was followed by cDNA synthesis using the High-Capacity cDNA Reverse Transcription Kit (Applied Biosystems). A Rotor-Gene Q instrument (Qiagen) was used to perform qPCR reactions using the Rotor-Gene SYBR Green Kit (Qiagen) with the following primers: AAATTCAAATGCTCCTGGGAT and GTTGAGCAAAAGCTCAGTTGT-GT for *slit*; CAATCGCTTCTACTTTGGCTTATC and ATATCCTCCATT-CAGTCCAATCTC for *Diptericin*; AGTACTTGTTCGCCCTCTTCG and CTTCGCACCAGCACTTCAGACT for *Drosomycin*; AAAAGCTTACAA-AATGTGTGACGA and CAATCGATGGGAAGACGG for *Actin 5C*. PCR assays were performed in triplicate. Relative expression data were normalized to *Actin 5C*.

Acknowledgements

We thank Sarolta Pálfia for technical assistance; Bruce Edgar, Heinrich Jasper, Yiorgos Apidianakis, Bruno Lemaitre and the Bloomington and Kyoto *Drosophila* Stock Centers for providing *Drosophila* lines; Csaba Sőti for providing pathogenic bacteria; and Jan Veenstra for antibodies.

Competing interests

The authors declare no competing or financial interests.

Author contributions

Conceptualization: P.N., Z.S., G.J.; Methodology: P.N., Z.S., G.O.S., M.L., K.H., G.J.; Formal analysis: P.N., Z.S., G.O.S.; Writing - original draft: P.N.; Writing - review & editing: P.N., Z.S., G.J.; Supervision: G.J.; Funding acquisition: P.N., K.H., G.J.

Funding

This work was supported by the Hungarian Academy of Sciences (Magyar Tudományos Akadémia; Momentum LP-2014/2 to G.J.); and the National Research, Development and Innovation Office (Nemzeti Kutatási, Fejlesztési és Innovációs Hivatal; PD115568 to P.N., PD112632 to K.H., and K119842, GINOP-2.3.2-15-2016-00032 to G.J.). P.N. is a Bolyai Scholar.

Supplementary information

Supplementary information available online at
http://dev.biologists.org/lookup/doi/10.1242/dev.147033.supplemental

References

Adolph, T. E., Tomczak, M. F., Niederreiter, L., Ko, H.-J., Böck, J., Martinez-Naves, E., Glickman, J. N., Tschurtschenthaler, M., Hartwig, J., Hosomi, S. et al. (2013). Paneth cells as a site of origin for intestinal inflammation. *Nature* **503**, 272-276.

Amcheslavsky, A., Jiang, J. and Ip, Y. T. (2009). Tissue damage-induced intestinal stem cell division in Drosophila. *Cell Stem Cell* **4**, 49-61.

Amcheslavsky, A., Song, W., Li, Q., Nie, Y., Bragatto, I., Ferrandon, D., Perrimon, N. and Ip, Y. T. (2014). Enteroendocrine cells support intestinal stem-cell-mediated homeostasis in Drosophila. *Cell Rep.* **9**, 32-39.

Anderson, C. A., Boucher, G., Lees, C. W., Franke, A., D'Amato, M., Taylor, K. D., Lee, J. C., Goyette, P., Imielinski, M., Latiano, A. et al. (2011). Meta-analysis identifies 29 additional ulcerative colitis risk loci, increasing the number of confirmed associations to 47. *Nat. Genet.* **43**, 246-252.

Azuara, D., Rodriguez-Moranta, F., de Oca, J., Sanjuan, X., Guardiola, J., Lobaton, T., Wang, A., Boadas, J., Piqueras, M., Monfort, D. et al. (2013). Novel methylation panel for the early detection of neoplasia in high-risk ulcerative colitis and Crohn's colitis patients. *Inflamm. Bowel Dis.* **19**, 165-173.

Beehler-Evans, R. and Micchelli, C. A. (2015). Generation of enteroendocrine cell diversity in midgut stem cell lineages. *Development* **142**, 654-664.

Biteau, B. and Jasper, H. (2014). Slit/Robo signaling regulates cell fate decisions in the intestinal stem cell lineage of Drosophila. *Cell Rep.* **7**, 1867-1875.

Biteau, B., Hochmuth, C. E. and Jasper, H. (2008). JNK activity in somatic stem cells causes loss of tissue homeostasis in the aging Drosophila gut. *Cell Stem Cell* **3**, 442-455.

Boada-Romero, E., Serramito-Gómez, I., Sacristán, M. P., Boone, D. L., Xavier, R. J. and Pimentel-Muiños, F. X. (2016). The T300A Crohn's disease risk polymorphism impairs function of the WD40 domain of ATG16L1. *Nat. Commun.* **7**, 11821.

Buchon, N., Osman, D., David, F. P., Fang, H. Y., Boquete, J.-P., Deplancke, B. and Lemaitre, B. (2013). Morphological and molecular characterization of adult midgut compartmentalization in Drosophila. *Cell Rep.* **3**, 1725-1738.

Cadwell, K., Liu, J. Y., Brown, S. L., Miyoshi, H., Loh, J., Lennerz, J. K., Kishi, C., Kc, W., Carrero, J. A., Hunt, S. et al. (2008). A key role for autophagy and the autophagy gene Atg16l1 in mouse and human intestinal Paneth cells. *Nature* **456**, 259-263.

Carmona, F. J., Azuara, D., Berenguer-Llergo, A., Fernandez, A. F., Biondo, S., de Oca, J., Rodriguez-Moranta, F., Salazar, R., Villanueva, A., Fraga, M. F. et al. (2013). DNA methylation biomarkers for noninvasive diagnosis of colorectal cancer. *Cancer Prev. Res.* **6**, 656-665.

Chen, J., Kim, S. M. and Kwon, J. Y. (2016). A systematic analysis of Drosophila regulatory peptide expression in enteroendocrine cells. *Mol. Cells* **39**, 358-366.

Chugani, S. A., Whiteley, M., Lee, K. M., D'Argenio, D., Manoil, C. and Greenberg, E. P. (2001). QscR, a modulator of quorum-sensing signal synthesis and virulence in Pseudomonas aeruginosa. *Proc. Natl. Acad. Sci. USA* **98**, 2752-2757.

Coe, B. P., Witherspoon, K., Rosenfeld, J. A., van Bon, B. W. M., Vulto-van Silfhout, A. T., Bosco, P., Friend, K. L., Baker, C., Buono, S., Vissers, L. E. et al. (2014). Refining analyses of copy number variation identifies specific genes associated with developmental delay. *Nat. Genet.* **46**, 1063-1071.

Deuring, J. J., Fuhler, G. M., Konstantinov, S. R., Peppelenbosch, M. P., Kuipers, E. J., de Haar, C. and van der Woude, C. J. (2014). Genomic ATG16L1 risk allele-restricted Paneth cell ER stress in quiescent Crohn's disease. *Gut* **63**, 1081-1091.

Dutta, D., Dobson, A. J., Houtz, P. L., Gläßer, C., Revah, J., Korzelius, J., Patel, P. H., Edgar, B. A. and Buchon, N. (2015). Regional cell-specific transcriptome mapping reveals regulatory complexity in the adult Drosophila midgut. *Cell Rep.* **12**, 346-358.

Ekbom, A., Helmick, C., Zack, M. and Adami, H.-O. (1990). Increased risk of large-bowel cancer in Crohn's disease with colonic involvement. *Lancet* **336**, 357-359.

Fujita, N., Saitoh, T., Kageyama, S., Akira, S., Noda, T. and Yoshimori, T. (2009). Differential involvement of Atg16L1 in Crohn disease and canonical autophagy: analysis of the organization of the Atg16L1 complex in fibroblasts. *J. Biol. Chem.* **284**, 32602-32609.

Fujita, N., Morita, E., Itoh, T., Tanaka, A., Nakaoka, M., Osada, Y., Umemoto, T., Saitoh, T., Nakatogawa, H., Kobayashi, S. et al. (2013). Recruitment of the autophagic machinery to endosomes during infection is mediated by ubiquitin. *J. Cell Biol.* **203**, 115-128.

Gillingham, A. K., Sinka, R., Torres, I. L., Lilley, K. S. and Munro, S. (2014). Toward a comprehensive map of the effectors of rab GTPases. *Dev. Cell* **31**, 358-373.

Grimm, W. A., Messer, J. S., Murphy, S. F., Nero, T., Lodolce, J. P., Weber, C. R., Logsdon, M. F., Bartulis, S., Sylvester, B. E., Springer, A. et al. (2016). The Thr300Ala variant in ATG16L1 is associated with improved survival in human colorectal cancer and enhanced production of type I interferon. *Gut* **65**, 456-464.

Hampe, J., Franke, A., Rosenstiel, P., Till, A., Teuber, M., Huse, K., Albrecht, M., Mayr, G., De La Vega, F. M., Briggs, J. et al. (2007). A genome-wide association scan of nonsynonymous SNPs identifies a susceptibility variant for Crohn disease in ATG16L1. *Nat. Genet.* **39**, 207-211.

Hegedűs, K., Takats, S., Boda, A., Jipa, A., Nagy, P., Varga, K., Kovacs, A. L. and Juhasz, G. (2016). The Ccz1-Mon1-Rab7 module and Rab5 control distinct steps of autophagy. *Mol. Biol. Cell* **27**, 3132-3142.

Huttenhower, C., Kostic, A. D. and Xavier, R. J. (2014). Inflammatory bowel disease as a model for translating the microbiome. *Immunity* **40**, 843-854.

Jiang, H. and Edgar, B. A. (2012). Intestinal stem cell function in Drosophila and mice. *Curr. Opin. Genet. Dev.* **22**, 354-360.

Jiang, H., Patel, P. H., Kohlmaier, A., Grenley, M. O., McEwen, D. G. and Edgar, B. A. (2009). Cytokine/Jak/Stat signaling mediates regeneration and homeostasis in the Drosophila midgut. *Cell* **137**, 1343-1355.

Jiang, T., Qin, B., He, J., Lin, S. and Ding, S. (2013). Three isoforms of the Atg16L1 protein contribute different autophagic properties. *Mol. Cell. Biochem.* **378**, 257-266.

Juhasz, G., Erdi, B., Sass, M. and Neufeld, T. P. (2007). Atg7-dependent autophagy promotes neuronal health, stress tolerance, and longevity but is dispensable for metamorphosis in Drosophila. *Genes Dev.* **21**, 3061-3066.

Kim, M., Sandford, E., Gatica, D., Qiu, Y., Liu, X., Zheng, Y., Schulman, B. A., Xu, J., Semple, I., Ro, S. H. et al. (2016). Mutation in ATG5 reduces autophagy and leads to ataxia with developmental delay. *Elife* **5**, e12245.

Development (2017) 144, 3990-4001 doi:10.1242/dev.147033

Kini, A. T., Thangaraj, K. R., Simon, E., Shivappagowdar, A., Thiagarajan, D., Abbas, S., Ramachandran, A. and Venkatraman, A. (2015). Aberrant Niche signaling in the etiopathogenesis of ulcerative colitis. *Inflamm. Bowel Dis.* **21**, 2549-2561.

Kuballa, P., Huett, A., Rioux, J. D., Daly, M. J. and Xavier, R. J. (2008). Impaired autophagy of an intracellular pathogen induced by a Crohn's disease associated ATG16L1 variant. *PLoS ONE* **3**, e3391.

Lassen, K. G., Kuballa, P., Conway, K. L., Patel, K. K., Becker, C. E., Peloquin, J. M., Villablanca, E. J., Norman, J. M., Liu, T.-C., Heath, R. J. et al. (2014). Atg16L1 T300A variant decreases selective autophagy resulting in altered cytokine signaling and decreased antibacterial defense. *Proc. Natl. Acad. Sci. USA* **111**, 7741-7746.

Li, H. and Jasper, H. (2016). Gastrointestinal stem cells in health and disease: from flies to humans. *Dis. Model. Mech.* **9**, 487-499.

Lobatón, T., Azuara, D., Rodriguez-Moranta, F., Loayza, C., Sanjuan, X., de Oca, J., Fernandez-Robles, A., Guardiola, J. and Capella, G. (2014). Relationship between methylation and colonic inflammation in inflammatory bowel disease. *World J. Gastroenterol.* **20**, 10591-10598.

Lőrincz, P., Tóth, S., Benkő, P., Lakatos, Z., Boda, A., Glatz, G., Zobel, M., Bisi, S., Hegedűs, K., Takáts, S. et al. (2017). Rab2 promotes autophagic and endocytic lysosomal degradation. *J. Cell Biol.* **216**, 1937-1947.

Matsushita, M., Suzuki, N. N., Obara, K., Fujioka, Y., Ohsumi, Y. and Inagaki, F. (2007). Structure of Atg5·Atg16, a complex essential for autophagy. *J. Biol. Chem.* **282**, 6763-6772.

McGovern, D. P., Kugathasan, S. and Cho, J. H. (2015). Genetics of inflammatory bowel diseases. *Gastroenterology* **149**, 1163-1176.e2.

Murthy, A., Li, Y., Peng, I., Reichelt, M., Katakam, A. K., Noubade, R., Roose-Girma, M., DeVoss, J., Diehl, L., Graham, R. R. et al. (2014). A Crohn's disease variant in Atg16l1 enhances its degradation by caspase 3. *Nature* **506**, 456-462.

Nagy, P., Varga, A., Pircs, K., Hegedűs, K. and Juhász, G. (2013). Myc-driven overgrowth requires unfolded protein response-mediated induction of autophagy and antioxidant responses in Drosophila melanogaster. *PLoS Genet.* **9**, e1003664.

Nagy, P., Varga, A., Kovács, A. L., Takáts, S. and Juhász, G. (2015). How and why to study autophagy in Drosophila: it's more than just a garbage chute. *Methods* **75**, 151-161.

Nagy, P., Kovács, L., Sándor, G. O. and Juhász, G. (2016). Stem-cell-specific endocytic degradation defects lead to intestinal dysplasia in Drosophila. *Dis. Model. Mech.* **9**, 501-512.

Neyen, C., Bretscher, A. J., Binggeli, O. and Lemaitre, B. (2014). Methods to study Drosophila immunity. *Methods* **68**, 116-128.

Nezis, I. P., Simonsen, A., Sagona, A. P., Finley, K., Gaumer, S., Contamine, D., Rusten, T. E., Stenmark, H. and Brech, A. (2008). Ref(2)P, the Drosophila melanogaster homologue of mammalian p62, is required for the formation of protein aggregates in adult brain. *J. Cell Biol.* **180**, 1065-1071.

Noda, N. N. and Inagaki, F. (2015). Mechanisms of autophagy. *Annu. Rev. Biophys.* **44**, 101-122.

Pankiv, S., Clausen, T. H., Lamark, T., Brech, A., Bruun, J.-A., Outzen, H., Øvervatn, A., Bjørkøy, G. and Johansen, T. (2007). p62/SQSTM1 binds directly to Atg8/LC3 to facilitate degradation of ubiquitinated protein aggregates by autophagy. *J. Biol. Chem.* **282**, 24131-24145.

Pircs, K., Nagy, P., Varga, A., Venkei, Z., Erdi, B., Hegedus, K. and Juhasz, G. (2012). Advantages and limitations of different p62-based assays for estimating autophagic activity in Drosophila. *PLoS ONE* **7**, e44214.

Rioux, J. D., Xavier, R. J., Taylor, K. D., Silverberg, M. S., Goyette, P., Huett, A., Green, T., Kuballa, P., Barmada, M. M., Datta, L. W. et al. (2007). Genome-wide association study identifies new susceptibility loci for Crohn disease and implicates autophagy in disease pathogenesis. *Nat. Genet.* **39**, 596-604.

Saitoh, T., Fujita, N., Jang, M. H., Uematsu, S., Yang, B.-G., Satoh, T., Omori, H., Noda, T., Yamamoto, N., Komatsu, M. et al. (2008). Loss of the autophagy protein Atg16L1 enhances endotoxin-induced IL-1beta production. *Nature* **456**, 264-268.

Sallé, J., Gervais, L., Boumard, B., Stefanutti, M., Siudeja, K. and Bardin, A. J. (2017). Intrinsic regulation of enteroendocrine fate by Numb. *EMBO J.* **36**, 1928-1945.

Sartor, R. B. (2008). Therapeutic correction of bacterial dysbiosis discovered by molecular techniques. *Proc. Natl. Acad. Sci. USA* **105**, 16413-16414.

Sato, T., van Es, J. H., Snippert, H. J., Stange, D. E., Vries, R. G., van den Born, M., Barker, N., Shroyer, N. F., van de Wetering, M. and Clevers, H. (2011). Paneth cells constitute the niche for Lgr5 stem cells in intestinal crypts. *Nature* **469**, 415-418.

Schuldiner, O., Berdnik, D., Levy, J. M., Wu, J. S., Luginbuhl, D., Gontang, A. C. and Luo, L. (2008). piggyBac-based mosaic screen identifies a postmitotic function for cohesin in regulating developmental axon pruning. *Dev. Cell* **14**, 227-238.

Sinka, R., Gillingham, A. K., Kondylis, V. and Munro, S. (2008). Golgi coiled-coil proteins contain multiple binding sites for Rab family G proteins. *J. Cell Biol.* **183**, 607-615.

Swidsinski, A., Ladhoff, A., Pernthaler, A., Swidsinski, S., Loening-Baucke, V., Ortner, M., Weber, J., Hoffmann, U., Schreiber, S., Dietel, M. et al. (2002). Mucosal flora in inflammatory bowel disease. *Gastroenterology* **122**, 44-54.

Takáts, S., Nagy, P., Varga, A., Pircs, K., Kárpáti, M., Varga, K., Kovács, A. L., Hegedűs, K. and Juhasz, G. (2013). Autophagosomal Syntaxin17-dependent lysosomal degradation maintains neuronal function in Drosophila. *J. Cell Biol.* **201**, 531-539.

Varga, K., Nagy, P., Arsikin Csordás, K., Kovács, A. L., Hegedűs, K. and Juhász, G. (2016). Loss of Atg16 delays the alcohol-induced sedation response via regulation of Corazonin neuropeptide production in Drosophila. *Sci. Rep.* **6**, 34641.

Veenstra, J. A., Agricola, H.-J. and Sellami, A. (2008). Regulatory peptides in fruit fly midgut. *Cell Tissue Res.* **334**, 499-516.

Zavodszky, E., Vicinanza, M. and Rubinsztein, D. C. (2013). Biology and trafficking of ATG9 and ATG16L1, two proteins that regulate autophagosome formation. *FEBS Lett.* **587**, 1988-1996.

Zeng, X., Han, L., Singh, S. R., Liu, H., Neumüller, R. A., Yan, D., Hu, Y., Liu, Y., Liu, W., Lin, X. et al. (2015). Genome-wide RNAi screen identifies networks involved in intestinal stem cell regulation in Drosophila. *Cell Rep.* **10**, 1226-1238.

Supplemental information

Supplemental Figures and legends

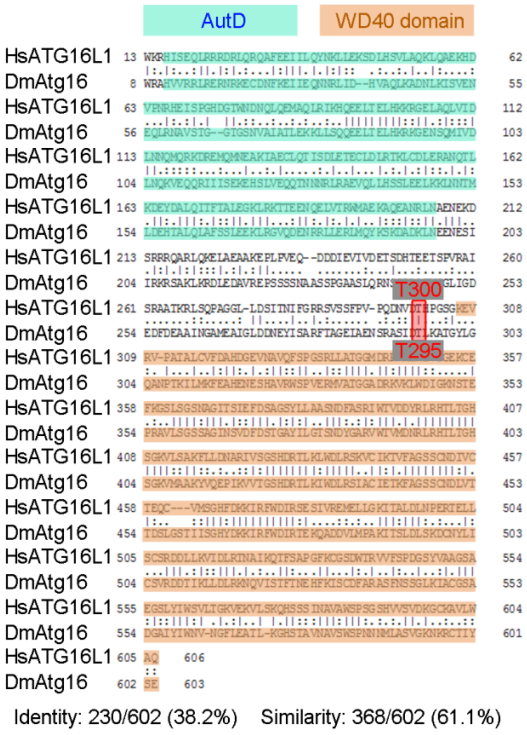

Fig. S1: Protein sequence alignment of human Atg16L1 and *Drosophila* Atg16. Identical protein regions and the position of human T300 and fly T295 are highlighted, based on homology between human Atg16L1 and fly Atg16 isoform C (the only Atg16 isoform that is expressed in the intestine, see Fig. S2A).

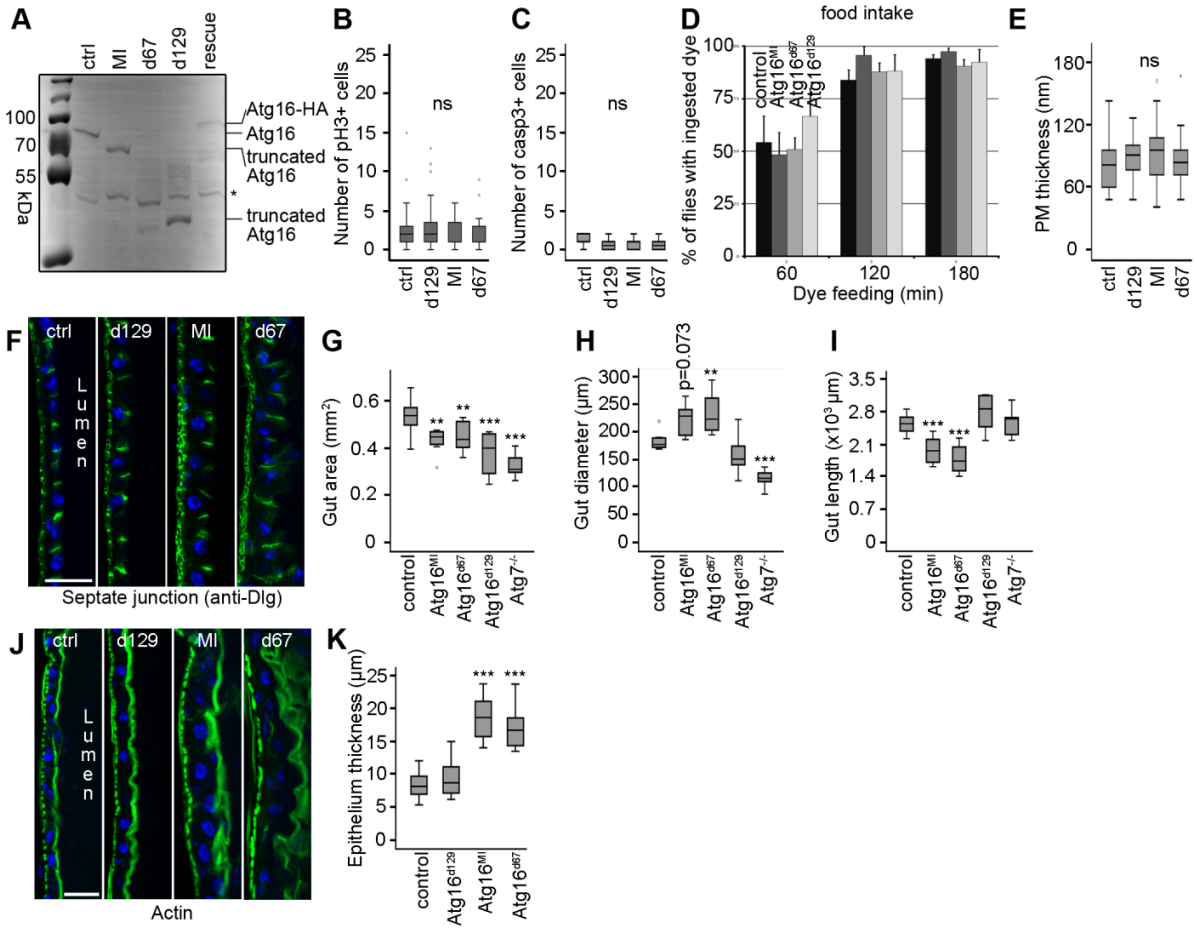

Fig. S2: Gut architecture and physiology is altered in Atg16 WD40 mutants. (A) Atg16 expression in gut protein extracts from different mutants and genetically rescued flies. Asterisk marks a non-specific band that serves as loading control. (B, C) The number of mitotic (B, N=8-9) and active caspase-3 positive apoptotic (C, N=5-6) cells does not change in 5-day-old control and *Atg16* mutant guts, Kruskal-Wallis tests. (D) Time course analysis of flies with ingested blue dye-containing food reveals no difference in feeding activity in the indicated *Atg16* mutants and controls. N=115-120, ANOVA. (E) Quantification of peritrophic membrane (PM) thickness from ultrastructural images. N=3, ANOVA. (F) Distribution and number of septate junctions marked by anti-Dlg appears similar in controls and different *Atg16* mutant intestinal walls. (G-I) Measurements of gut area (G, N=7-10, ANOVA), diameter (H, N=7-12, ANOVA) and length (I, N=7-13, ANOVA) in controls and *Atg16* mutants. (J) Anti-Actin staining shows the thickening of the gut epithelium in $Atg16^{MI}$ and $Atg16^{d67}$ mutant intestines compared

to control and *Atg16*^{d129} mutants, quantified in K. N=15, ANOVA. ** and *** represent p<0.05 and p<0.001 in G, H, I, K, respectively. Bars: 20 µm (F, J).

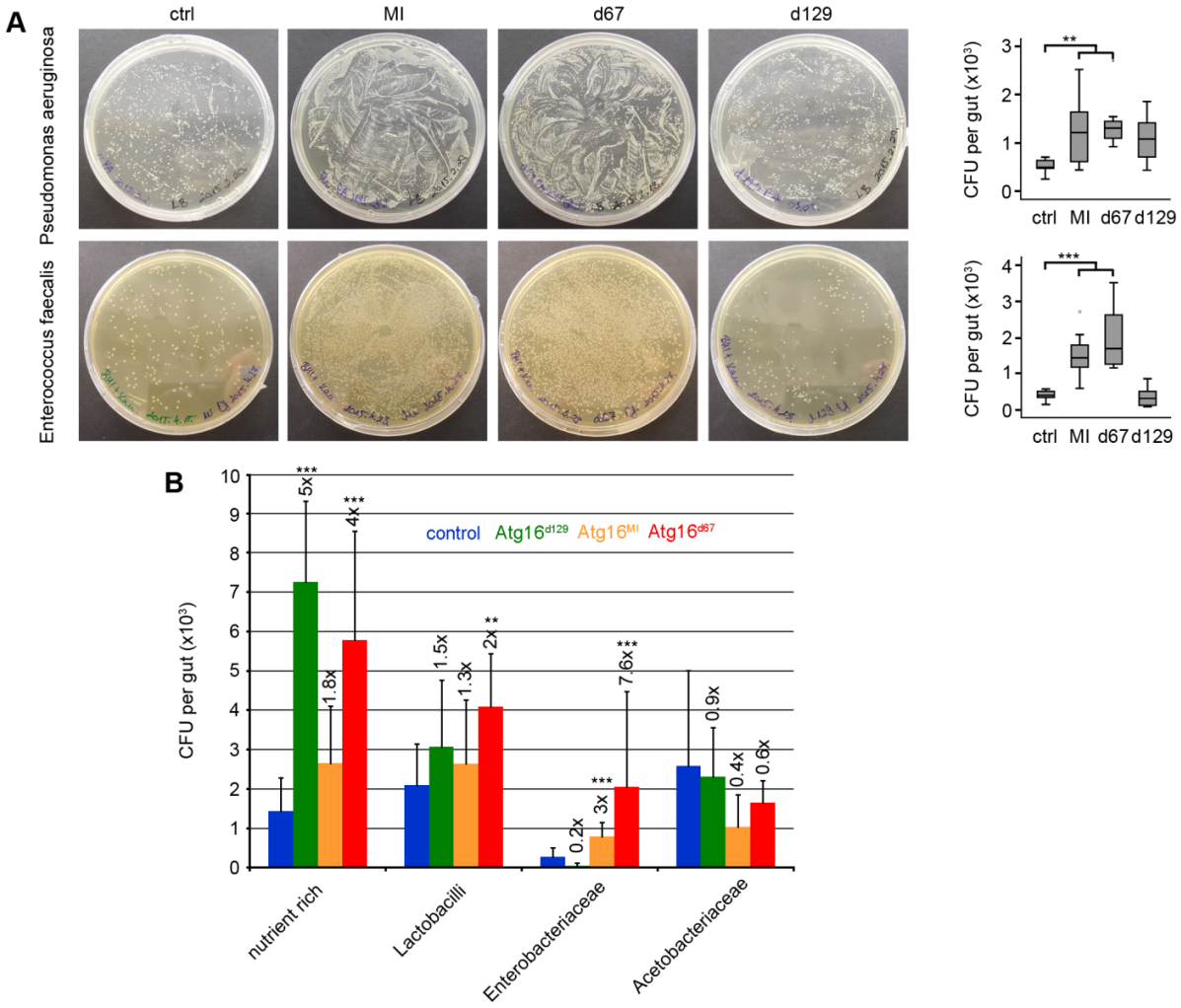

Fig. S3: Intestinal bacteria numbers change in *Atg16* mutant guts. (A) Representative images of bacteria derived from isolated and plated single guts following PA (N=10, ANOVA) and EF (N=9-10, ANOVA) oral infections. (B) Differential alterations in intestinal microbiota in various *Atg16* mutants. Numbers indicate fold change compared to the control in colony forming units (CFUs). N=7-11, ANOVA. ** and *** represent $p<0.05$ and $p<0.001$ in A, B, respectively.

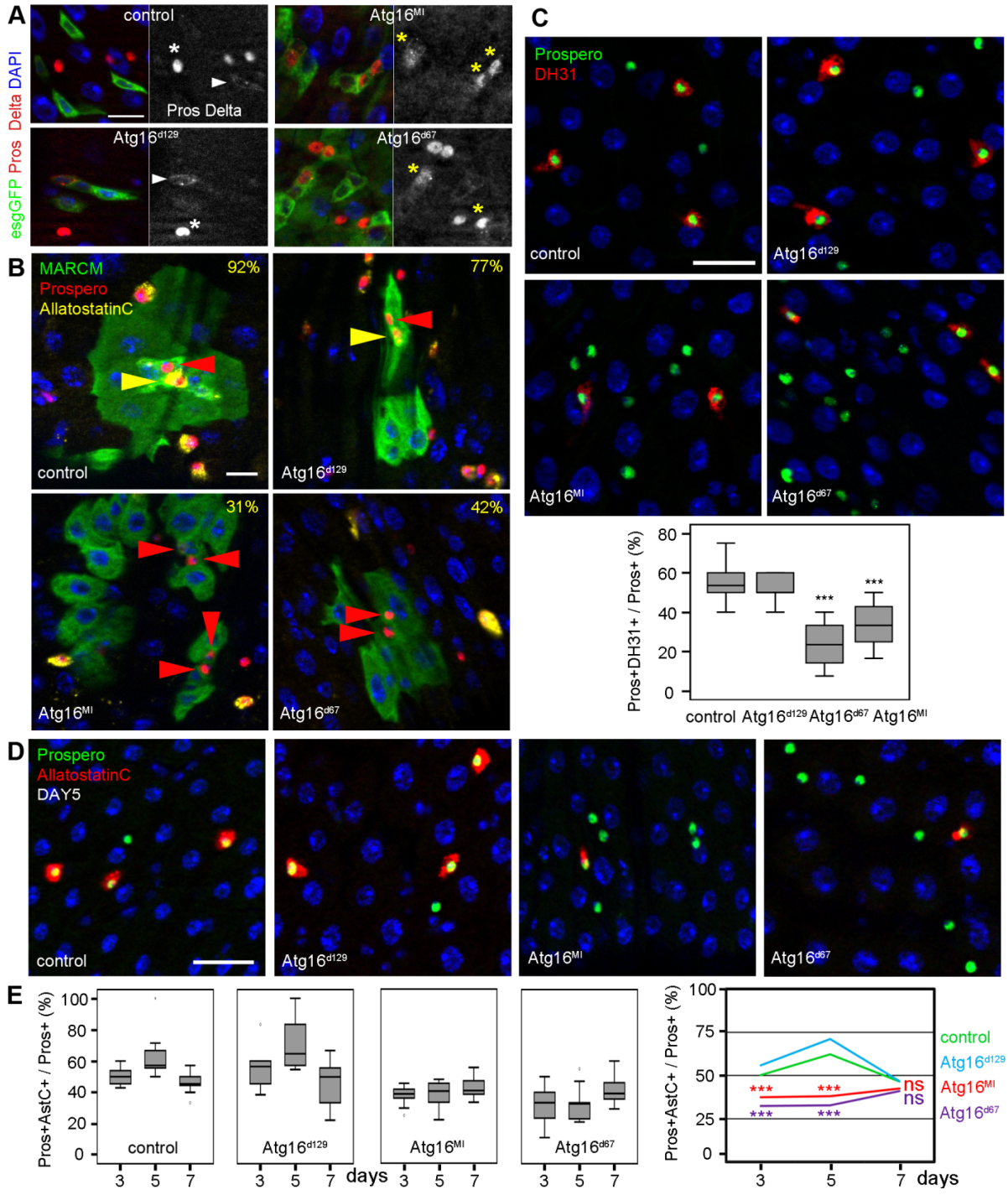

Fig. S4: Regulatory peptide expression in *Atg16* mutant guts. (A) Prospero and Delta co-label esgGFP+ pre-EEs in *Atg16*^{MI} and *Atg16*^{d67} mutant intestines. Arrowheads point to esgGFP+ Delta+ ISCs, white and yellow asterisks mark esgGFP+ Prospero+ and esgGFP+ Delta+ Prospero+ EE and preEE cells, respectively. (B) AllatostatinC (AstC) expression in different *Atg16* mutant clones. Yellow arrowheads indicate AstC-

producing Prospero+ mature EE cells, and red arrowheads point to Prospero+ cells that show no AstC expression. % refers to the average ratio of Pros+ AstC+ / all Pros+ cells within clones in the different genotypes, indicating a decrease of mature EEs in *Atg16*^{Ml} and *Atg16*^{d67} mutant clones. (C) The ratio of DH31-producing Prospero+ cells declines in *Atg16*^{Ml} and *Atg16*^{d67} mutant guts compared to controls, while it does not change in *Atg16*^{d129} mutants. N=10, ***: $p<0.001$, ANOVA. (D) Fewer AstC-producing Prospero+ cells are seen in *Atg16*^{Ml} and *Atg16*^{d67} mutant guts compared to controls, while it does not change in *Atg16*^{d129} mutants. (E) Time course analysis of the ratio of AstC-producing Prospero+ mature EE cells reveals a delay in EE differentiation in *Atg16*^{Ml} and *Atg16*^{d67} mutant guts compared to controls, while it does not change in *Atg16*^{d129} mutants. N=5, ***: $p<0.001$, ANOVA. Bars: 20 μm (A, C, D), 10 μm (B).

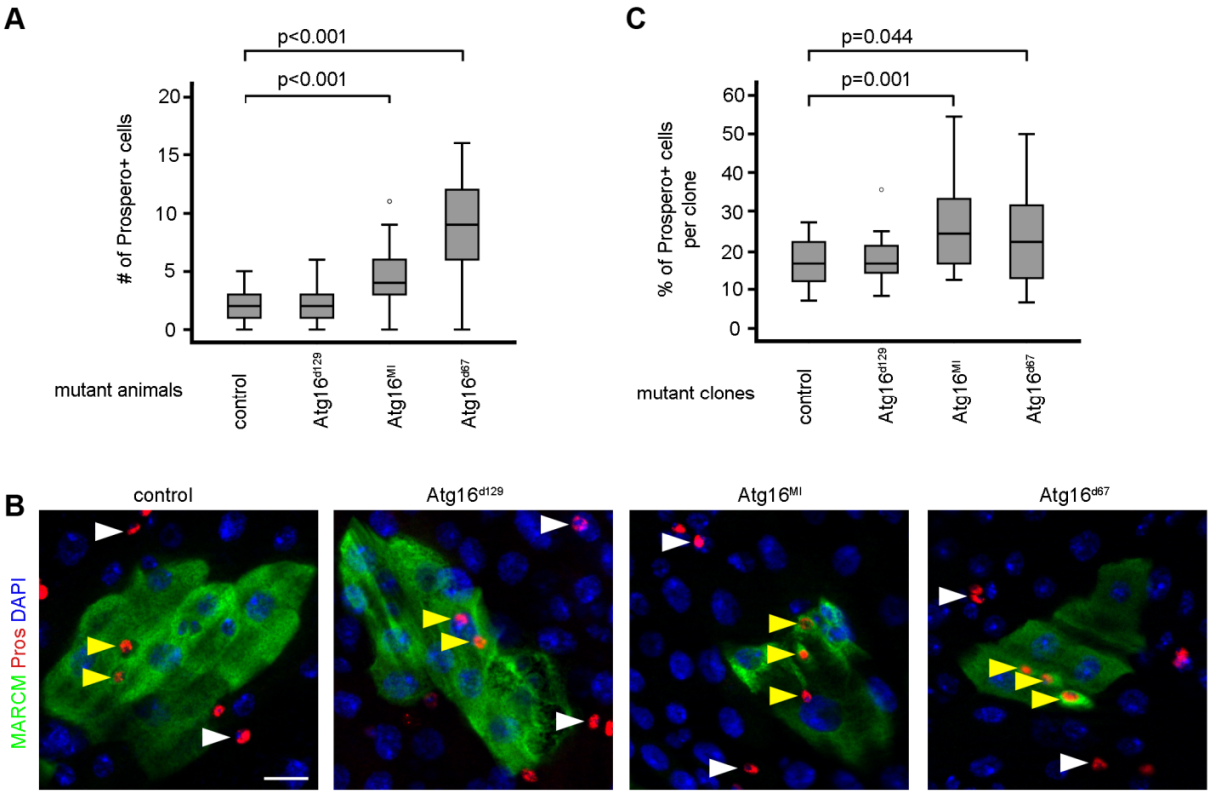

Fig. S5: Atg16 promotes EE differentiation. (A) Quantification of all Prospero-positive cells in *Atg16* mutants that are shown in Fig. 2C-F. N=6-12, Kruskal-Wallis test. (B) Prospero-positive (pre)-EE cell numbers increase in *Atg16^{MI}* and *Atg16^{d67}* mutant clones in mosaic intestines, as the percentage of Prospero+ cells in GFP-marked cell clones is higher than in control clones. Yellow arrowheads show Prospero-positive cells within the clones, white arrowheads indicate such cells outside of the clones. (C) Quantification of data. N=10, ANOVA. Bar: 20 µm (B).

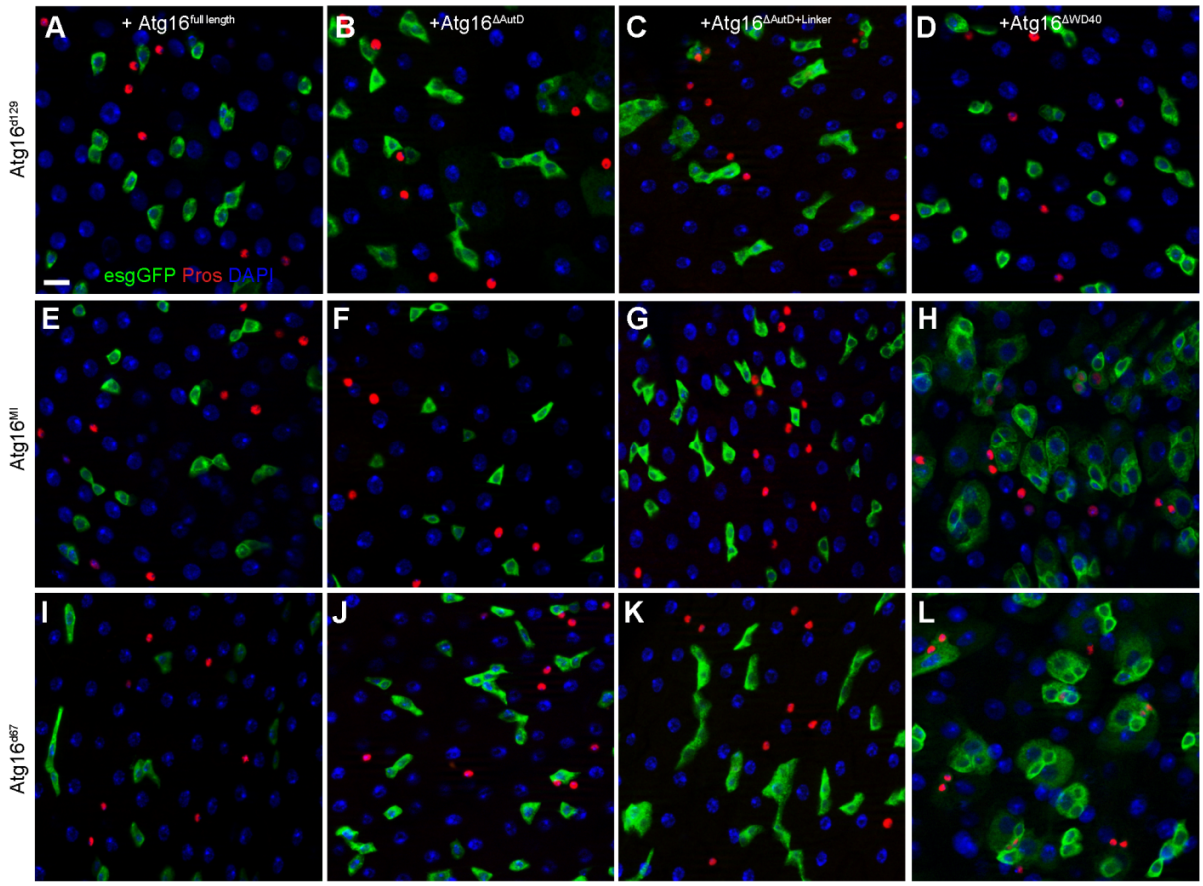

Fig. S6: Atg16 WD40 domain restores EE differentiation in WD40 mutants. Esg-specific overexpression of Atg16$^{\text{full length}}$ (E, I), Atg16$^{\Delta AutD}$ (F, J) and Atg16$^{\Delta AutD+Linker}$ (G, K) rescues the EE cell differentiation defect of *Atg16^{MI}* and *Atg16^{d67}* mutant intestines, while these genetic manipulations have no effect on EE cells in the *Atg16^{d129}* mutant (A-D). Esg-specific overexpression Atg16$^{\Delta WD40}$ does not affect EE differentiation status in *Atg16* mutants (D, H, L). See Fig. 2G for quantification of data. Bar: 10 µm (A-L).

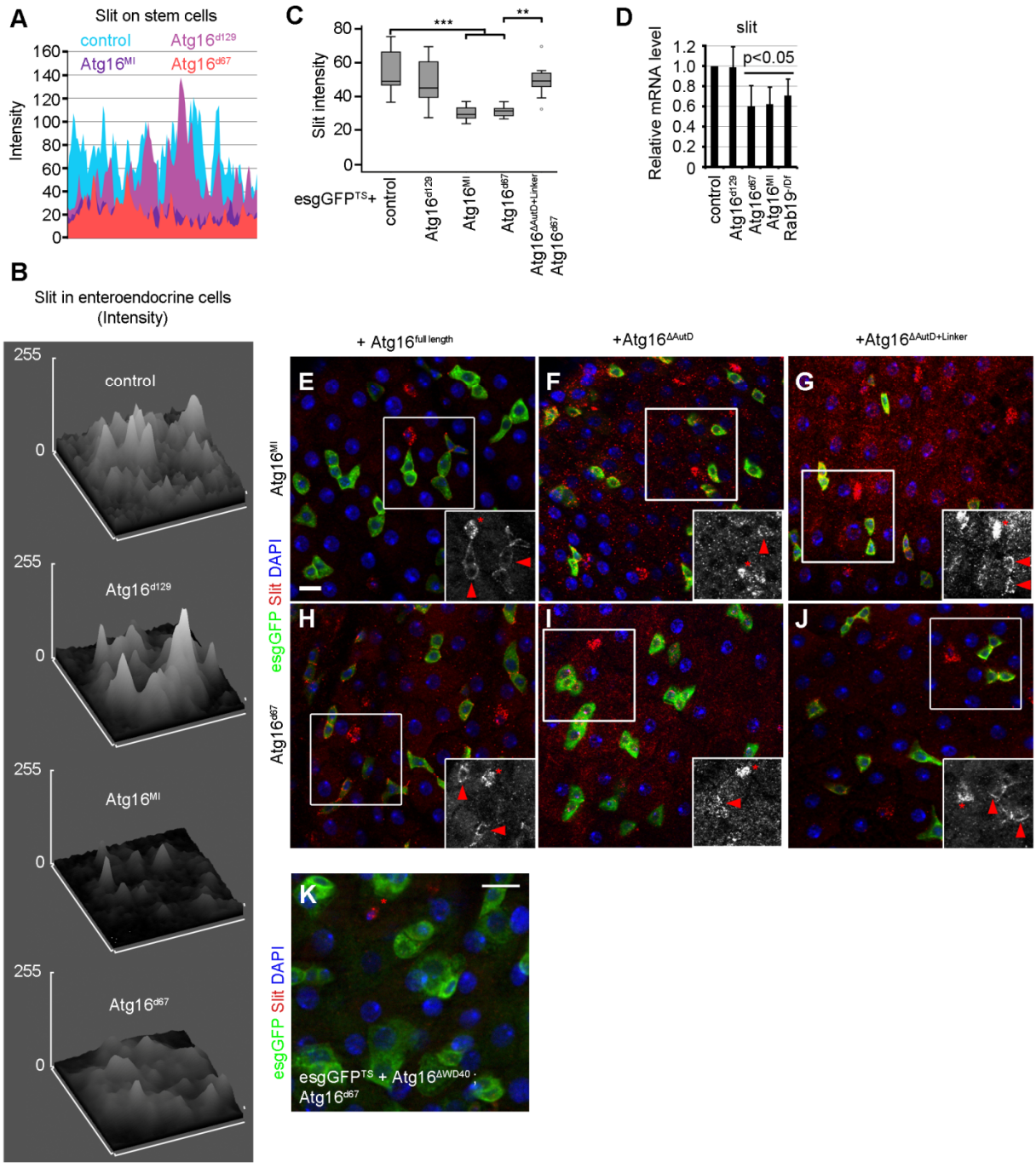

Fig. S7: Atg16 WD40 domain promotes Slit/Robo signaling. (A) Histogram shows overall Slit intensity on intestinal stem cells in wild type and different *Atg16* mutants. (B) Surface plot profiles of Slit intensity in Prospero-positive cells of wild-type and *Atg16* mutants. (C) Slit staining intensity decreases in $Atg16^{MI}$ and $Atg16^{d67}$ intestines, which is fully restored by WD40 domain ($Atg16^{\Delta AutD+Linker}$) overexpression in $Atg16^{d67}$ mutants.

N=10, ***: p<0.001, **: p<0.01, ANOVA. (D) Slit mRNA expression decreases in *Atg16*^{MI}, *Atg16*^{d67} and *Rab19* mutant intestines compared to controls, whereas it does not change in *Atg16*^{d129} mutant guts. (E-J) Esg-specific overexpression of Atg16$^{\text{full length}}$ (E and H), Atg16$^{\Delta\text{AutD}}$ (F and I) and Atg16$^{\Delta\text{AutD+Linker}}$ (G and J) restores Slit production in EE cells and Slit localization on stem cells in *Atg16*^{MI} (E-G) and *Atg16*^{d67} (H-J) mutant intestines, respectively. (K) Escargot-specific overexpression of Atg16$^{\Delta\text{WD40}}$ does not restore Slit production in *Atg16*^{d67} mutants. Red asterisks indicate Slit-producing EE cells in E-K, while red arrowheads show Slit localization on stem cells in E-J. Bar: 10 μm (E-J), 20 μm (K).

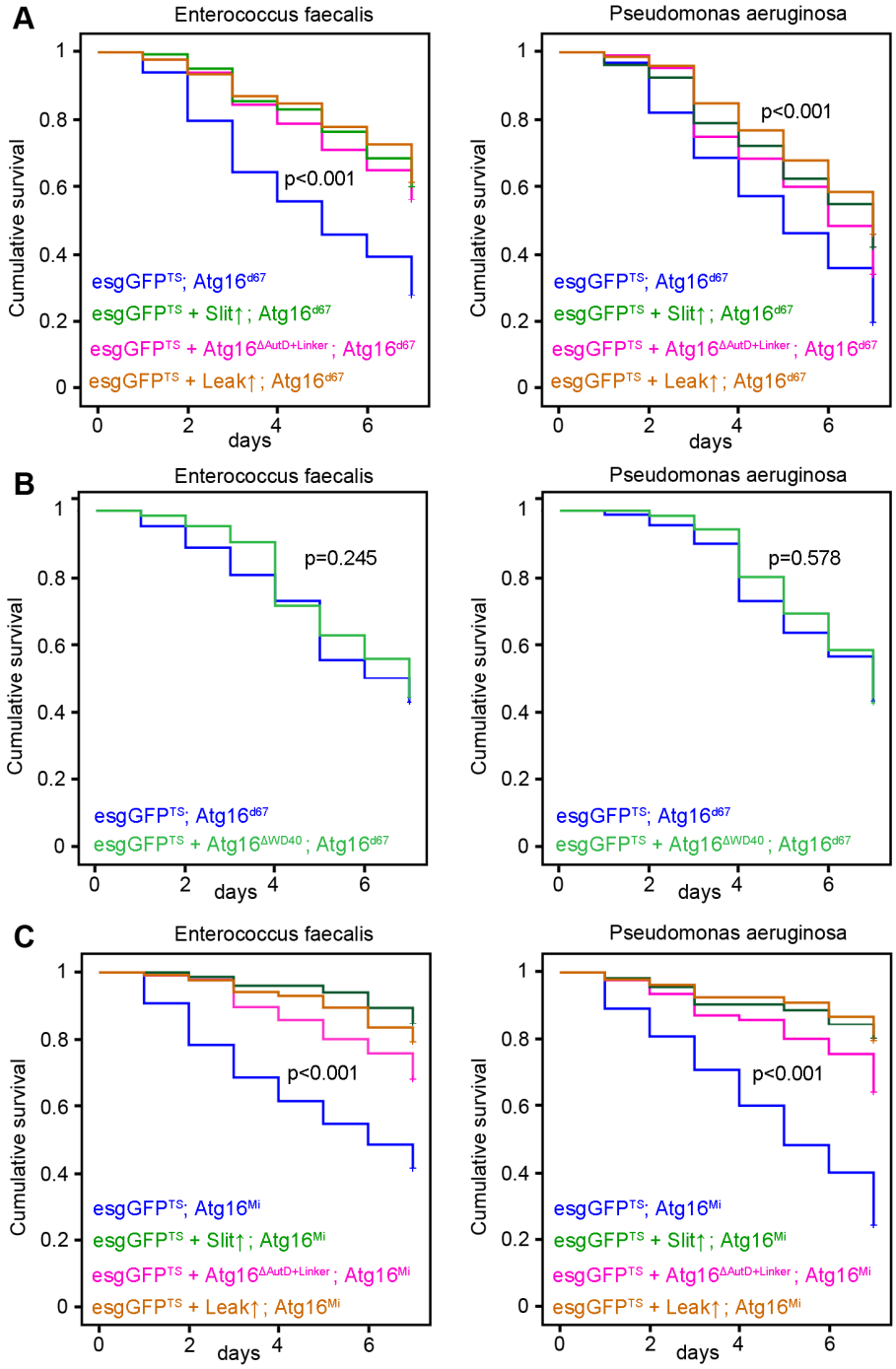

Fig. S8: Slit, Robo2 and Atg16 WD40 domain overexpression improves the resistance of WD40 mutants to bacterial infection. (A, C) Esg-specific overexpression of Slit, Atg16 WD40 domain ($Atg16^{\Delta AutD+Linker}$) and Leak/Robo2 increases resistance to oral bacterial infection with EF and PA in *Atg16*^{d67} (A) and *Atg16*^{Ml} (C) mutant flies. Kaplan-Meier survival curves are shown, p-values are

calculated by Log-rank analyses. (B) Esg-specific overexpression of Atg16$^{\Delta WD40}$ in *Atg16^{d67}* mutants does not improve resistance to oral infection by PA or EF. Kaplan-Meier survival curves are shown, and p-values were calculated by Log-rank analyses. N=166-344 (EF) and N=133-290 (PA) for panel A, N=395-509 (EF) and N=424-508 (PA) for panel B, N=152-339 (EF) and N=116-280 (PA) for panel C.

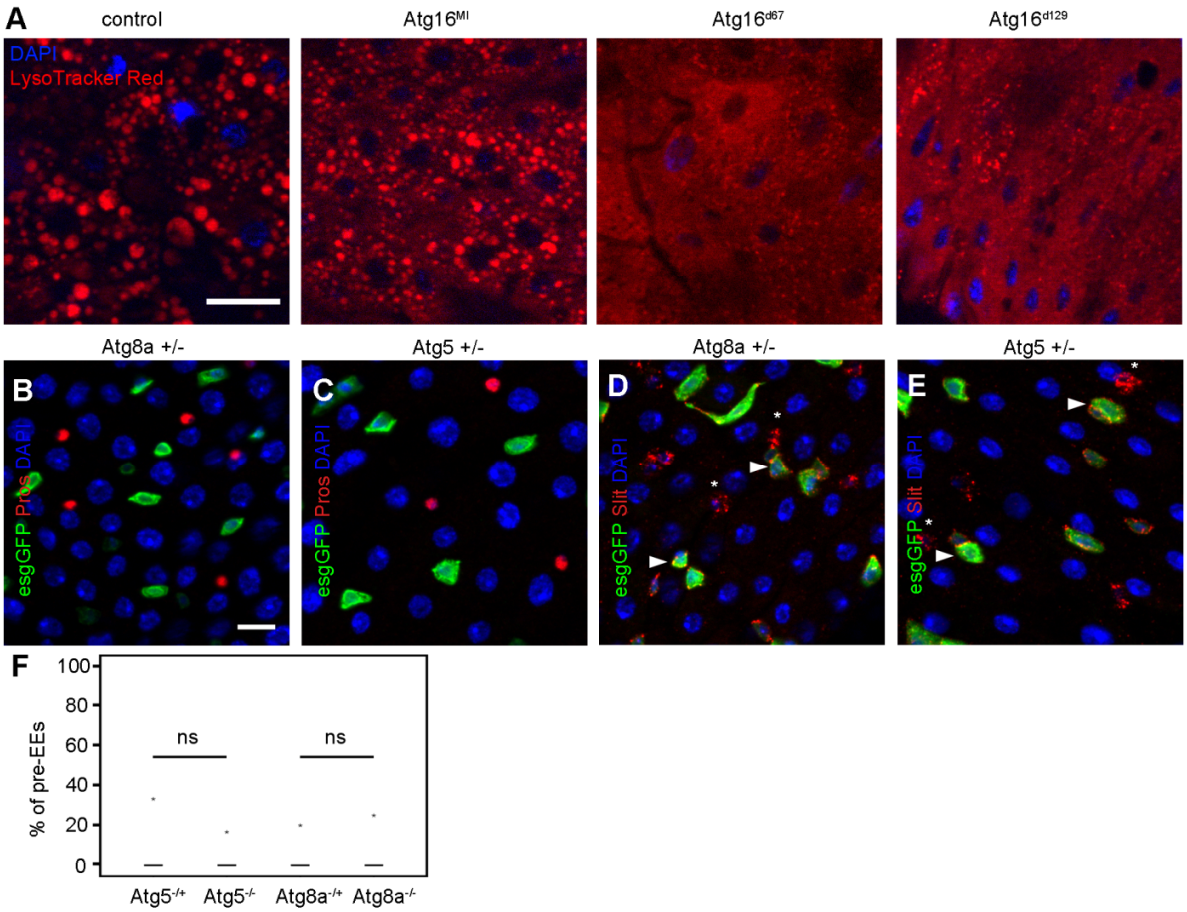

Fig. S9: Autophagy in *Atg16* mutants and EE differentiation in *Atg5* and *Atg8a* heterozygotes. (A) Acidic compartments labeled by LysoTracker Red decrease in *Atg16*^{d129} and *Atg16*^{d67} autophagy mutant midguts compared to control and *Atg16*^{MI} mutant animals. (B-E) *Atg8a* and *Atg5* heterozygous midguts do not show any cell differentiation or Slit localization defects. (F) Quantification of Prospero+ esgGFP+ / total Prospero+ cell data from panels B, C (genotype controls) and Fig. 6K, L (homozygous *Atg8a* and *Atg5* mutants). N=5, two-tailed two-sample T tests. Bar: 20 µm (A), 10 µm (B).

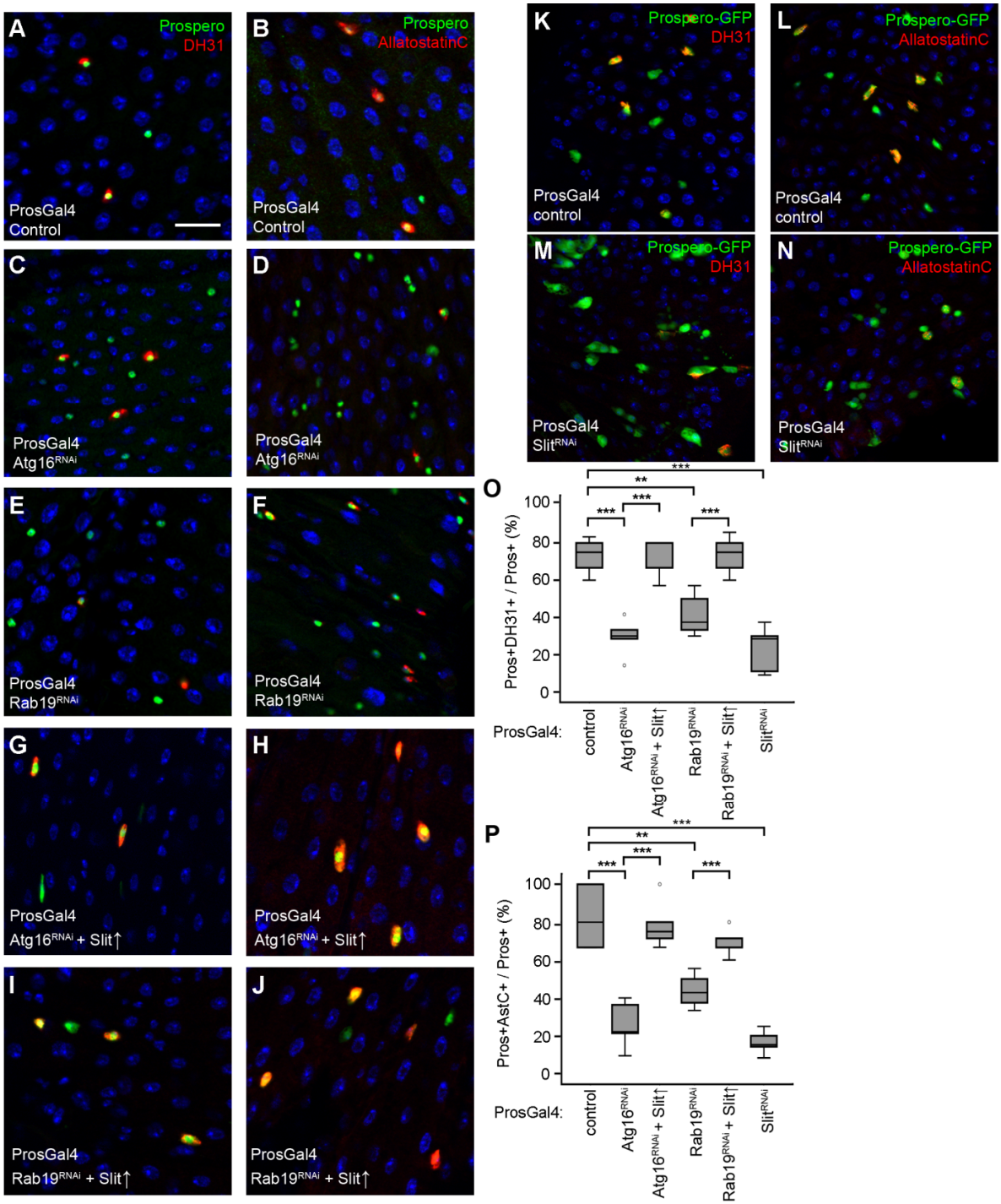

Fig. S10: EE lineage-specific knockdown of *Atg16* or *Rab19* perturbs peptide hormone secretion in a Slit-dependent manner

Expression of DH31 (A) and AllatostatinC (B) in control midguts. Prospero-specific *Atg16* (C, D) or *Rab19* (E, F) RNAi decreases the ratio of Prospero-positive cells

producing DH31 and AllatostatinC. (H). Overexpression of Slit (G-J) restores peptide hormone expression in *Atg16 (*G, H) and *Rab19* (I, J) RNAi cells. RNAi silencing of *slit* decreases the ratio of DH31-positive EE cells (M) compared to controls (K). Similarly, knockdown of *slit* decreases the ratio of AllatostatinC-positive EE cells (N) compared to controls (L). Prospero-positive cells were labeled by anti-Pros for A-J and by anti-GFP for K-N. Quantification of data from A, C, E, G, I, K, M (O) and B, D, F, H, J, L, N (P). The last quarter of the posterior midgut was sampled for DH31 and the first half of the posterior midgut was sampled for AstC, respectively, because we detected highest peptide expression in those subregions. N=5, ***: $p<0.001$, **: $p<0.01$, based on ANOVA for both O and P. Bar: 20 µm for A-N.

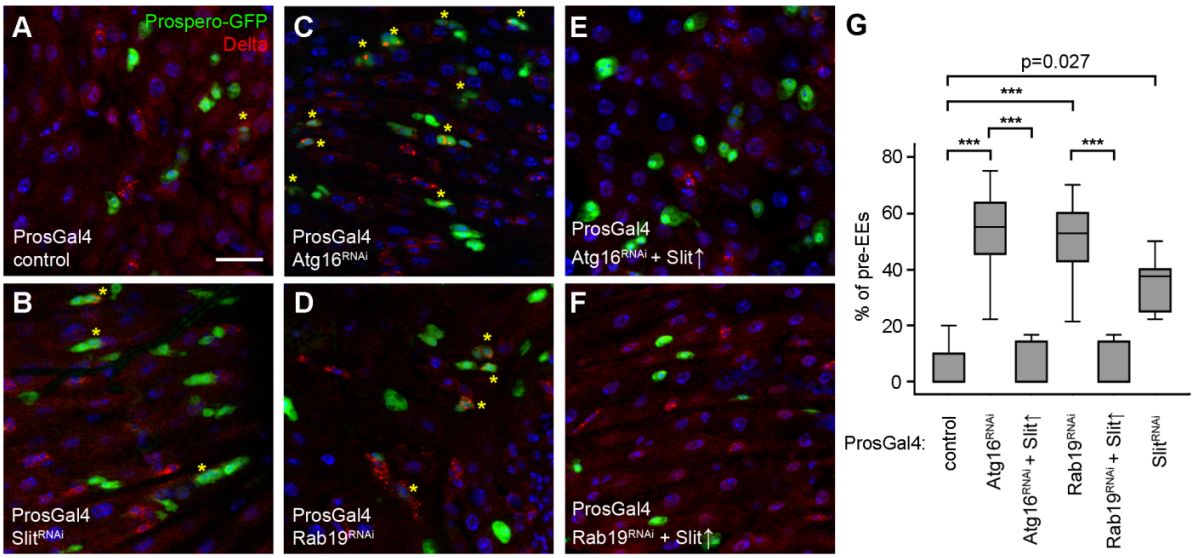

Fig. S11: EE lineage-specific knockdown of *Atg16* or *Rab19* perturbs EE differentiation in a Slit-dependent manner

Pre-EEs positive for both Prospero and Delta (asterisk) are rarely detected in control midguts (A). Prospero-specific knockdown of *slit* (B), *Atg16* (C) or *Rab19* (D) increases the ratio of pre-EEs containing both Prospero and Delta. Overexpression of Slit restores pre-EE cell number in Prospero-specific *Atg16* (E) and *Rab19* (F) RNAi guts. (G) Quantification of data. N=5, ***: p<0.001, Kruskal-Wallis test. Bar: 20 µm for A-F.